

# Comparison of Roe-type methods for solving the two-fluid model with and without pressure relaxation\*

Svend Tollak Munkejord<sup>†</sup>

*Norwegian University of Science and Technology (NTNU),  
Department of Energy and Process Engineering,  
Kolbjørn Hejes veg 1A, NO-7491 Trondheim, Norway*

## Abstract

Two strategies for the numerical resolution of a two-fluid model have been investigated. Both methods employ a Roe-type scheme. The first method (Roe4) solves the four-equation, one-pressure, isentropic two-fluid model directly.

The second strategy (Roe5) is to add an evolution equation for the volume fraction. In the present case, that results in a five-equation two-pressure model, where it is necessary to employ pressure relaxation to calculate the typical two-phase problems that have been tested: The water faucet and two benchmark shock-tube problems known from the literature.

The numerical calculations showed that the Roe4 and Roe5 schemes converge to the same solution when instantaneous pressure relaxation is employed in the Roe5 scheme. This is true both with and without the use of high-resolution flux-limiter functions. However, the Roe5 scheme was found to be significantly more diffusive than the Roe4 scheme. The diffusion is a strong function of the chosen time-step length, the grid size, whether a limiter function is employed or not, and also the liquid speed of sound.

As the pressure-relaxation parameter in the Roe5 scheme was increased, the solution gradually approached that obtained using instantaneous pressure relaxation.

Furthermore, the results indicate that the approach of two pressures and instantaneous pressure relaxation does not provide an easy way to overcome the problem of complex eigenvalues in the one-pressure two-fluid model.

*Keywords:* Two-phase flow, Roe-type methods, pressure relaxation, compressible flow

---

\*Date: 2007-10-28. Preprint of an article published in *Computers & Fluids*, vol. 36, no. 6, 2007.

<sup>†</sup>E-mail: stm@pvv.ntnu.no

## 1 Introduction

For the numerical solution of flow models, the approximate Riemann solver of Roe (1981) is an attractive candidate, since it provides an upwind resolution of all wave phenomena inherent in the models, and as it requires only the solution of a linear Riemann problem at each cell interface. Among the problems encountered for the two-fluid model, is the complicated eigenstructure, as well as the appearance of non-conservative terms (Toumi, 1996).

Sainsaulieu (1995) introduced a Roe-type Riemann solver for the case of incompressible liquid droplets suspended in a gas, that is, for small liquid volume fractions. More general configurations were considered by Toumi (1996), and a Roe-type method for the isentropic two-fluid model was presented by Toumi and Kumbaro (1996). However, also in the latter works, the liquid density was assumed to be constant. That assumption was not used in the method by Eyje and Flåtten (2003).

A different approach has been to consider two-pressure models, whose mathematical properties have been found preferable (Ransom and Hicks, 1984). On the other hand, for many cases, the latter kind of methods needs a *pressure-relaxation* procedure.

Saurel and Abgrall (1999) presented a two-velocity two-pressure two-phase model of seven equations, where pressure and / or velocity relaxation could be performed after the hyperbolic time step. The model can be thought of as an extension of that of Baer and Nunziato (1986). It was expanded to several space dimensions by Saurel and LeMetayer (2001), and it was stated to be suitable for compressible multiphase flows with interfaces, shocks, detonation waves and cavitation. Murrone and Guillard (2005) discussed a five-equation diffuse interface model where the two phases had common pressures and velocities. Different pressure-relaxation procedures were tested by Lallemand *et al.* (2005).

The approximate Riemann solver employed by Saurel and Abgrall (1999) was a modified Harten, Lax and van Leer (HLL) scheme. Other authors have later presented similar methods using other solvers. Niu (2001) applied a modified advection upstream splitting method (AUSMD) and solved the seven-equation model in one and two dimensions, also adding a  $k-\varepsilon$  turbulence model. A Roe-type scheme for the seven-equation model was presented by Karni *et al.* (2004).

In this work, we perform a *direct comparison* between a one-pressure four-equation approach, and a two-pressure five-equation approach, employing a Roe-type method in each case. A priori, both strategies have advantages. For the five-equation system, simple, analytical expressions for the eigenvalues and eigenvectors are available. On the other hand, the four-equation system has one less equation to be solved. Only the five-equation system can be used if the physical system to be modelled has two independent pressures. Here we explore the effect of varying pressure-relaxation parameter in the five-equation system.

Section 2 briefly describes the two-fluid model formulation, including constitutive relations. In Section 3, the equation systems are written in characteristic form, and the Roe matrices are detailed. The Roe method is described in Section 4. In Section 5, numerical tests are performed. Finally, in Section 6, the main conclusions are drawn.

## 2 Model formulation

This section briefly presents the employed four-equation two-fluid model, the five-equation formulation, including pressure relaxation, as well as the constitutive relations.

### 2.1 Four-equation system

The one-dimensional, inviscid, isentropic multiphase flow is customarily described by the continuity equation

$$\frac{\partial}{\partial t}(\alpha_k \rho_k) + \frac{\partial}{\partial x}(\alpha_k \rho_k u_k) = 0, \quad (1)$$

and the momentum equation

$$\frac{\partial}{\partial t}(\alpha_k \rho_k u_k) + \frac{\partial}{\partial x}(\alpha_k \rho_k u_k^2) + \alpha_k \frac{\partial p_k}{\partial x} + (p_k - p_{ik}) \frac{\partial \alpha_k}{\partial x} = \alpha_k \rho_k g_x, \quad (2)$$

when mass transfer, wall friction, interface friction, and other possible effects are neglected. In practical applications, one or more of these effects can be important. In the numerical study presented here, on the other hand, we wish to focus on the mathematically essential parts of the two-fluid model, keeping the number of parameters low. Such a practise is common (see e.g. Abgrall and Saurel, 2003; Evje and Flåtten, 2003; Cortes *et al.*, 1998) and facilitates a comparison of results obtained by different researchers.

Due to the term  $p_{ik} \partial \alpha_k / \partial x$ , the equation system cannot be written in conservation form in terms of the variables  $\alpha_k \rho_k$  and  $\alpha_k \rho_k u_k$ . Therefore, special care is needed for the spatial discretization of the system.

In addition to the above equations, an equation of state (EOS) is needed. Here we take

$$p_k = c_k^2(\rho_k - \rho_k^\circ), \quad (3)$$

where the speed of sound,  $c_k$ , and the ‘reference density’,  $\rho_k^\circ$ , are constants for each phase. In this work we consider two phases, air and water, with the properties given in Table 1. These values correspond to the ones used by Evje and Flåtten (2003). The equation of state (3) with constant coefficients is an implicit assumption of isothermal flow. This can be shown using basic thermodynamic

relations (see e.g. Munkejord, 2005). As can be seen from Toumi (1996), the entropy waves are advected with the fluid velocities, that is, they are uncoupled from the remaining wave structure, which can therefore be studied by considering an isentropic model.

Moreover, an expression is needed for the relation between the pressures in the phases, for example

$$p_k = p_l + \sigma_{kl} \quad \forall k \neq l, \quad (4)$$

where  $\sigma_{kl}$  is a constant pertaining to the relation between the phases  $k$  and  $l$ . In this work we shall take  $\sigma_{kl} = 0$ . Finally, of course, a relation for the interfacial pressure  $p_{ik}$  must be specified.

The equation system that has been described in this subsection will be called the *four-equation system*.

## 2.2 Five-equation system

It is natural to assume that the volume fraction  $\alpha_k$  is advected with the flow, that is

$$\frac{\partial \alpha_k}{\partial t} + u_{ik} \frac{\partial \alpha_k}{\partial x} = 0, \quad (5)$$

where  $u_{ik}$  is the average interface velocity of phase  $k$ . Equation (5) is the ensemble-average (see Drew and Passman, 1999, Section 11.2) of the topological equation derived by Drew and Passman (1999, Section 9.1.3). It can be added to the basic-equations system (1)–(2), as was similarly done by Saurel and Abgrall (1999); Baer and Nunziato (1986).

### 2.2.1 Interfacial-velocity models

Some model has to be specified for the average interface velocity, which is the ‘grad  $\alpha$ -weighted’ average of the local interface velocity  $\mathbf{v}_{ik}$ :

$$u_{ik} = \frac{\mathcal{E}(\mathbf{v}_{ik} \cdot \nabla \chi_k)}{\partial \alpha_k / \partial x}, \quad (6)$$

where  $\chi$  is the phase-indicator function (characteristic function),  $\mathcal{E}(\cdot)$  denotes the ensemble-averaging operator, and the volume fraction is given by

$$\alpha_k = \mathcal{E}(\chi_k). \quad (7)$$

Table 1: Constants in the equation of state

	$c_k$ (m/s)	$\rho_k^\circ$ (kg/m <sup>3</sup> )
air (g)	$\sqrt{10^5}$	0
water ( $\ell$ )	1000	999.9

Saurel and Abgrall (1999) took the average interface velocity to be the mass-weighted velocity:

$$u_{ik} = u_i = \frac{\sum_{\forall k} \alpha_k \rho_k u_k}{\sum_{\forall k} \alpha_k \rho_k}. \quad (8)$$

This will be the default model in the present work.

### 2.2.2 Pressure relaxation

When the energy equation is disregarded, the Saurel and Abgrall model can be written as

$$\frac{\partial \alpha_g}{\partial t} + u_i \frac{\partial \alpha_g}{\partial x} = r_p (p_g - p_\ell), \quad (9)$$

$$\frac{\partial}{\partial t} (\alpha_k \rho_k) + \frac{\partial}{\partial x} (\alpha_k \rho_k u_k) = 0, \quad (10)$$

$$\frac{\partial}{\partial t} (\alpha_k \rho_k u_k) + \frac{\partial}{\partial x} (\alpha_k \rho_k u_k^2) + \alpha_k \frac{\partial p_k}{\partial x} + (p_k - p_{ik}) \frac{\partial \alpha_k}{\partial x} = s_k + r_u (u_l - u_k). \quad (11)$$

Herein,  $s_k$  is a momentum-source term. The parameters  $r_u$  and  $r_p$  deserve some attention.  $r_u$  is a velocity-relaxation parameter, and a large value of  $r_u$  will force equality of the two phasic velocities. In this work we shall not consider velocity relaxation, and henceforth

$$r_u \equiv 0. \quad (12)$$

$r_p$  is a pressure-relaxation parameter. It is the inverse of the compaction viscosity discussed by Baer and Nunziato (1986), something which can be confirmed by checking that the unit of  $r_p$  is the inverse of that of the molecular viscosity. For  $r_p = 0$ , the two phasic pressures are linearly independent, and when  $r_p \rightarrow \infty$ , they are equal.

The system (9)-(11) with (12) will be referred to as the *five-equation system*.

With the addition of the equation (9) to the system, the condition (4) is no longer needed. However, for many two-phase flows, including the ones considered here, the phasic pressures are not independent. This dependence is accounted for by the *pressure-relaxation procedure*. That procedure was discussed by Saurel and Abgrall (1999) for the full seven-equation system. Here the situation is somewhat simpler, since the energy equation is not considered.

**Finite pressure relaxation** Since the source term in the equation (9) may be large, it is necessary to solve the five-equation system using a suitable numerical method. Here, we employ a fractional-step method: First, the ‘hyperbolic part’ of

the system (9)–(11) (that is, with  $r_p \equiv 0$ ) is advanced one step,  $\Delta t$ , in time using a method to be described in the following. Next, the ‘relaxation part’ is considered:

$$\frac{\partial \alpha_g}{\partial t} = r_p(p_g - p_\ell), \quad (13)$$

$$\frac{\partial}{\partial t}(\alpha_k \rho_k) = 0, \quad (14)$$

$$\frac{\partial}{\partial t}(\alpha_k \rho_k u_k) = 0. \quad (15)$$

With the solution from the hyperbolic step as initial condition, the above system can be also be advanced one step  $\Delta t$  in time, using an ODE solver. The resulting solution is then passed to the hyperbolic solver for the next time step, etc.

**Instantaneous pressure relaxation** Specific values for the pressure-relaxation parameter  $r_p$  are most often unknown. However, the assumption of equal phasic pressures is widespread. Such situations can be catered for by setting  $r_p$  to a large value. However, instead of solving the system (13)–(15) of differential equations, it is numerically more efficient to solve the problem directly. After the hyperbolic operator has been applied, the volume fraction is modified so as to render the two pressures equal, keeping  $\alpha_k \rho_k$  and  $\alpha_k \rho_k u_k$  constant. This leads to a second-degree equation with positive solution

$$\alpha_\ell = \frac{-\psi_2 - \sqrt{\psi_2^2 - 4\psi_1\psi_3}}{2\psi_1}, \quad (16)$$

where

$$\psi_1 = c_\ell^2 \rho_\ell^\circ - c_g^2 \rho_g^\circ, \quad (17)$$

$$\psi_2 = -c_\ell^2(\alpha_\ell \rho_\ell + \rho_\ell^\circ) + c_g^2(-\alpha_g \rho_g + \rho_g^\circ), \quad (18)$$

and

$$\psi_3 = c_\ell^2 \alpha_\ell \rho_\ell. \quad (19)$$

When solving the five-equation system, we will be employing instantaneous pressure relaxation, unless otherwise stated. For the case of instantaneous pressure relaxation, the volume-fraction equation (9) becomes singular. A difference between the phasic pressures would then cause an immediate change in the volume fraction so as to render the pressures equal. Since the rest of the five-equation system is equal to the four-equation system, the solution of the former should approach that of the latter. Indeed, it is hypothesized that the five-equation system with instantaneous pressure relaxation can be regarded as providing an alternative numerical method for solving the four-equation two-fluid model.

### 2.3 Interfacial-pressure models

Several models for the interfacial pressure have been proposed in the literature. However, their physical content is often debatable.

The model of Soo (1990, pages 319–321) reads

$$p_k - p_{ik} = (1 - B_k)p_k, \quad (20)$$

where  $B_k$  is a ‘displacement factor’ close to unity, which can be regarded as a simplified model for forces causing dispersion of the volume-fraction profile, e.g. in intermittent flow.

Saurel and Abgrall (1999) suggested taking

$$p_k - p_{ik} = p_k - \sum_{\forall k} \alpha_k p_k \quad (21)$$

in conjunction with their seven-equation model. This seems like a reasonable first approximation. Unfortunately, it yields complex eigenvalues in the four-equation model.

In the CATHARE code, the following expression was employed for non-stratified flows (Bestion, 1990):

$$p_k - p_{ik} = \Delta p_{ik} = \gamma \frac{\alpha_g \alpha_\ell \rho_g \rho_\ell}{\alpha_g \rho_\ell + \alpha_\ell \rho_g} (u_g - u_\ell)^2, \quad (22)$$

where  $\gamma$  is a factor not appearing explicitly in Bestion (1990). It is remarkable that the above expression was employed without physical argumentation, but rather ‘simply to provide the hyperbolicity of the system’, which, indeed, it normally does, at least when there is slip between the phases, that is,  $(u_g - u_\ell)^2 \neq 0$ . On the other hand, the CATHARE expression has the redeeming feature that it approaches zero in the case of stagnant fluids, which seems reasonable when no surface-tension effects are accounted for. Because of this, and because it is commonly cited, the CATHARE model will be our default expression for the interfacial pressure difference, and we will take  $\gamma = 1.2$ , following Evje and Flåtten (2003), unless otherwise stated.

### 3 Characteristic form of the basic equations

To be able to employ the Roe method, we seek to write the system of transport equations in the following quasi-linear form:

$$\frac{\partial \mathbf{q}}{\partial t} + \mathbf{A}(\mathbf{q}) \frac{\partial \mathbf{q}}{\partial x} = \mathbf{s}(\mathbf{q}). \quad (23)$$

### 3.1 Characteristic form of the four-equation system

With

$$\mathbf{q} = [\alpha_g \rho_g \quad \alpha_\ell \rho_\ell \quad \alpha_g \rho_g u_g \quad \alpha_\ell \rho_\ell u_\ell]^T, \quad (24)$$

the coefficient matrix for the four-equation system can be shown to be

$$\mathbf{A}(\mathbf{q}) = \begin{bmatrix} 0 & 0 & 1 & 0 \\ 0 & 0 & 0 & 1 \\ \frac{\alpha_g \rho_\ell + \Delta p_{ig} \alpha_\ell / c_\ell^2}{\kappa} - u_g^2 & \frac{\alpha_g \rho_g - \Delta p_{ig} \alpha_g / c_g^2}{\kappa} & 2u_g & 0 \\ \frac{\alpha_\ell \rho_\ell + \Delta p_{i\ell} \alpha_\ell / c_\ell^2}{\kappa} & \frac{\alpha_\ell \rho_g + \Delta p_{i\ell} \alpha_g / c_g^2}{\kappa} - u_\ell^2 & 0 & 2u_\ell \end{bmatrix}, \quad (25)$$

where

$$\kappa = \alpha_\ell \rho_g / c_\ell^2 + \rho_\ell \alpha_g / c_g^2, \quad (26)$$

$$\Delta p_{ik} = p_k - p_{ik}. \quad (27)$$

The vector of source terms becomes

$$\mathbf{s} = [0 \quad 0 \quad \alpha_g \rho_g g_x \quad \alpha_\ell \rho_\ell g_x]^T. \quad (28)$$

It is unfeasible to derive exact closed-form expressions for the eigenvectors and eigenvalues of  $\mathbf{A}$ , and in the present calculations, they have therefore been found numerically.

### 3.2 Characteristic form of the five-equation system

#### 3.2.1 System matrix

For

$$\mathbf{q} = [\alpha_g \quad \alpha_g \rho_g \quad \alpha_g \rho_g u_g \quad \alpha_\ell \rho_\ell \quad \alpha_\ell \rho_\ell u_\ell]^T, \quad (29)$$

the coefficient matrix for the five-equation system has been found to be

$$\mathbf{A}(\mathbf{q}) = \begin{bmatrix} u_i & 0 & 0 & 0 & 0 \\ 0 & 0 & 1 & 0 & 0 \\ \Delta p_{ig} - \rho_g c_g^2 & c_g^2 - u_g^2 & 2u_g & 0 & 0 \\ 0 & 0 & 0 & 0 & 1 \\ -\Delta p_{i\ell} + \rho_\ell c_\ell^2 & 0 & 0 & c_\ell^2 - u_\ell^2 & 2u_\ell \end{bmatrix}, \quad (30)$$

with the source-term vector

$$\mathbf{s}(\mathbf{q}) = [0 \quad 0 \quad \alpha_g \rho_g g_x \quad 0 \quad \alpha_\ell \rho_\ell g_x]^T. \quad (31)$$

### 3.2.2 Eigenstructure and hyperbolicity

The matrix  $\mathbf{A}$  of the five-equation system has one advantage over its counterpart in Section 3.1 in that its eigenvalues are available as simple analytical expressions:

$$\boldsymbol{\lambda} = \left[ u_i \quad u_g - c_g \quad u_g + c_g \quad u_\ell - c_\ell \quad u_\ell + c_\ell \right]^T. \quad (32)$$

These eigenvalues are always real, and moreover, they are mostly distinct, except for the ‘transonic difficulty’ when one of the phasic velocities passes through the phasic speed of sound. The eigenvector matrix,  $\mathbf{R}$ , with the right eigenvectors  $\mathbf{r}_i$  of  $\mathbf{A}$  as its columns, was found as

$$\mathbf{R} = \begin{bmatrix} 1 & 0 & 0 & 0 & 0 \\ -\frac{(-\Delta p_{ig} + \rho_g c_g^2)}{(u_g - u_i)^2 - c_g^2} & 1 & 1 & 0 & 0 \\ \frac{(-\Delta p_{ig} + \rho_g c_g^2) u_i}{(u_g - u_i)^2 - c_g^2} & \lambda_2 & \lambda_3 & 0 & 0 \\ \frac{(-\Delta p_{i\ell} + \rho_\ell c_\ell^2)}{(u_\ell - u_i)^2 - c_\ell^2} & 0 & 0 & 1 & 1 \\ \frac{(-\Delta p_{i\ell} + \rho_\ell c_\ell^2) u_i}{(u_\ell - u_i)^2 - c_\ell^2} & 0 & 0 & \lambda_4 & \lambda_5 \end{bmatrix}, \quad (33)$$

where  $\lambda_i$  is element  $i$  of the vector  $\boldsymbol{\lambda}$  in equation (32). Further, the eigenvector  $\mathbf{r}_i$  corresponds to the eigenvalue  $\lambda_i$ .

The matrix  $\mathbf{R}^{-1}$ , with the left eigenvectors  $\mathbf{l}_j^T$  of  $\mathbf{A}$  as its rows, is given by:

$$\mathbf{R}^{-1} = \begin{bmatrix} 1 & 0 & 0 & 0 & 0 \\ \frac{1}{2} \frac{(-\Delta p_{ig} + \rho_g c_g^2)}{(\lambda_2 - u_i) c_g} & \frac{1}{2} \frac{\lambda_3}{c_g} & -\frac{1}{2 c_g} & 0 & 0 \\ -\frac{1}{2} \frac{(-\Delta p_{ig} + \rho_g c_g^2)}{(\lambda_3 - u_i) c_g} & -\frac{1}{2} \frac{\lambda_2}{c_g} & \frac{1}{2 c_g} & 0 & 0 \\ -\frac{1}{2} \frac{(-\Delta p_{i\ell} + \rho_\ell c_\ell^2)}{(\lambda_4 - u_i) c_\ell} & 0 & 0 & \frac{1}{2} \frac{\lambda_5}{c_\ell} & -\frac{1}{2 c_\ell} \\ \frac{1}{2} \frac{(-\Delta p_{i\ell} + \rho_\ell c_\ell^2)}{(\lambda_5 - u_i) c_\ell} & 0 & 0 & -\frac{1}{2} \frac{\lambda_4}{c_\ell} & \frac{1}{2 c_\ell} \end{bmatrix}. \quad (34)$$

Since here the left eigenvectors are taken from from  $\mathbf{R}^{-1}$ , the left and the right eigenvectors are orthonormal:  $\mathbf{l}_i^T \mathbf{r}_j = \delta_{ij}$ .

For the five-equation system to be hyperbolic, the matrix  $\mathbf{A}$  must be diagonalizable with real eigenvalues. Therefore, the right eigenvectors  $\mathbf{r}_i$  must be linearly independent, and it is easy to show that  $\mathbf{r}_2, \mathbf{r}_3, \mathbf{r}_4$  and  $\mathbf{r}_5$  are so.  $\mathbf{r}_1$ , on the other hand, needs special attention. Ransom and Hicks (1984) studied a five-equation two-pressure two-fluid model whose coefficient matrix was mathematically analogous to the one considered here. They showed that the hyperbolicity depends on the quantities

$$\beta_k = -\Delta p_{ik} + \rho_k c_k^2, \quad (35)$$

and

$$\gamma_k = (u_k - u_i)^2 - c_k^2 \quad (36)$$

and they identified four cases, concerning the eigenvector  $\mathbf{r}_1$  associated with  $\lambda_1 = u_i$ :

1. When  $\gamma_g \neq 0$  and  $\gamma_\ell \neq 0$ , then  $\mathbf{r}_1$  as given by the equation (33) is linearly independent of the other eigenvectors for all values of  $\beta_g$  and  $\beta_\ell$ .
2. When  $\gamma_g = 0$  and  $\gamma_\ell \neq 0$ , then there exists a linearly independent  $\mathbf{r}_1$  if and only if  $\beta_g = 0$ . It is given by

$$\mathbf{r}_1 = \begin{bmatrix} 1 & 0 & 0 & \frac{(-\Delta p_{i\ell} + \rho_\ell c_\ell^2)}{(u_\ell - u_i)^2 - c_\ell^2} & \frac{(-\Delta p_{i\ell} + \rho_\ell c_\ell^2)u_i}{(u_\ell - u_i)^2 - c_\ell^2} \end{bmatrix}^T. \quad (37)$$

3. When  $\gamma_g \neq 0$  and  $\gamma_\ell = 0$ , then there exists a linearly independent  $\mathbf{r}_1$  if and only if  $\beta_\ell = 0$ . It is given by

$$\mathbf{r}_1 = \begin{bmatrix} 1 & -\frac{(-\Delta p_{ig} + \rho_g c_g^2)}{(u_g - u_i)^2 - c_g^2} & -\frac{(-\Delta p_{ig} + \rho_g c_g^2)u_i}{(u_g - u_i)^2 - c_g^2} & 0 & 0 \end{bmatrix}^T. \quad (38)$$

4. When  $\gamma_g = 0$  and  $\gamma_\ell = 0$ , then there exists a linearly independent  $\mathbf{r}_1$  if and only if  $\beta_g = 0$  and  $\beta_\ell = 0$ . It is given by

$$\mathbf{r}_1 = \begin{bmatrix} 1 & 0 & 0 & 0 & 0 \end{bmatrix}^T. \quad (39)$$

Here we mainly consider low-speed flows, and the restriction  $u_k \pm c_k \neq u_i$  is not thought to be of very much concern.

It is interesting to note that for the five-equation system, the interfacial pressure difference  $\Delta p_{ik}$  may very well be equal to zero. For the four-equation system, on the other hand, this quantity must not be too small. This can be shown by numerical experiments or analytical considerations (see e.g. Ramshaw and Trapp, 1978). As a result of this, several researchers have dedicated their efforts to inventing large-enough expressions for the interfacial pressure difference, leading, conveniently, to a diagonalizable  $\mathbf{A}$ . One example is Chung *et al.* (2002).

Since the relaxation terms in (9)-(11) do not contain derivatives of  $\mathbf{q}$ , the hyperbolicity of the five-equation system is not influenced by them. However, the case of instantaneous pressure relaxation might be interesting to study mathematically in more detail, but that is outside the scope of the present work.

## 4 A Roe-type method for solving the two-fluid model

In this section, a Roe-type method for the multiphase equations will be described.

### 4.1 Framework

A high-resolution extension of Godunov's method can be written as (LeVeque, 2002, Section 15.4)

$$\mathbf{Q}_i^{n+1} = \mathbf{Q}_i^n - \frac{\Delta t}{\Delta x} (\mathcal{A}^- \Delta \mathbf{Q}_{i+1/2} + \mathcal{A}^+ \Delta \mathbf{Q}_{i-1/2}) - \frac{\Delta t}{\Delta x} (\tilde{\mathbf{F}}_{i+1/2} - \tilde{\mathbf{F}}_{i-1/2}), \quad (40)$$

where  $\mathbf{Q}_i^n$  denotes the numerical approximation to the cell average of the vector of unknowns  $\mathbf{q}(x, t_n)$ , that is, in control volume  $i$  at time step  $n$ . Quantities without a time index are evaluated at time step  $n$ . The symbol  $\mathcal{A}^- \Delta \mathbf{Q}_{i+1/2}$  denotes the net effect of all left-going waves at  $x_{i+1/2}$ , that is, at the control-volume boundary midway between  $x_i$  and  $x_{i+1}$ , while  $\mathcal{A}^+ \Delta \mathbf{Q}_{i-1/2}$  measures the net effect of all right-going waves at  $x_{i-1/2}$ . The waves and wave speeds from the approximate Riemann solution are used to define

$$\begin{aligned} \mathcal{A}^- \Delta \mathbf{Q}_{i-1/2} &= \sum_{p=1}^m (s_{i-1/2}^p)^- \mathcal{W}_{i-1/2}^p, \\ \mathcal{A}^+ \Delta \mathbf{Q}_{i-1/2} &= \sum_{p=1}^m (s_{i-1/2}^p)^+ \mathcal{W}_{i-1/2}^p, \end{aligned} \quad (41)$$

where  $\mathcal{W}_{i-1/2}^p$  is the  $p$ th wave arising in the solution to the Riemann problem at  $x_{i-1/2}$ , that is, it is a vector with one component for each equation.  $m$  is the number of waves, and since we will be using a linearized Riemann solver, it is equal to the number of equations.  $s_{i-1/2}^p$  is the wave speed of the  $p$ th wave, and

$$(s_{i-1/2}^p)^+ = \max(s_{i-1/2}^p, 0), \quad (s_{i-1/2}^p)^- = \min(s_{i-1/2}^p, 0). \quad (42)$$

The flux vector  $\tilde{\mathbf{F}}_{i-1/2}$  is what LeVeque calls the high-resolution correction. It is given by

$$\tilde{\mathbf{F}}_{i-1/2} = \frac{1}{2} \sum_{p=1}^m |s_{i-1/2}^p| \left(1 - \frac{\Delta t}{\Delta x} |s_{i-1/2}^p|\right) \tilde{\mathcal{W}}_{i-1/2}^p, \quad (43)$$

where  $\widetilde{\mathcal{W}}_{i-1/2}^p$  is a limited version of the wave  $\mathcal{W}_{i-1/2}^p$ . With the correction terms, the method approaches second order in space and time for smooth solutions.

In the present work, we have taken account of source terms by adding the term  $\Delta t \mathbf{S}_i$  to the right-hand side of (40).

## 4.2 Roe linearization

The Roe (1981) linearization of conservation laws is well explained by LeVeque (2002, Section 15.3). Here some of the key points are repeated, after which the multifluid extension is presented.

### 4.2.1 Basic considerations

To define an approximate Riemann solution, the nonlinear problem

$$\frac{\partial \mathbf{q}}{\partial t} + \frac{\partial}{\partial x} \mathbf{f}(\mathbf{q}) = \mathbf{0} \quad (44)$$

is replaced by a linearized problem defined locally at each cell interface;

$$\frac{\partial \hat{\mathbf{q}}}{\partial t} + \hat{\mathbf{A}}_{i-1/2} \frac{\partial \hat{\mathbf{q}}}{\partial x} = \mathbf{0}. \quad (45)$$

For the Roe solver, we have the interpretation that

$$\mathcal{A}^\pm \Delta \mathbf{Q}_{i-1/2} = \hat{\mathbf{A}}_{i-1/2}^\pm (\mathbf{Q}_i - \mathbf{Q}_{i-1}). \quad (46)$$

Herein,

$$\hat{\mathbf{A}}_{i-1/2}^\pm = \hat{\mathbf{R}}_{i-1/2} \hat{\Lambda}_{i-1/2}^\pm \hat{\mathbf{R}}_{i-1/2}^{-1}, \quad (47)$$

where  $\hat{\mathbf{R}}_{i-1/2}$  is the matrix having the right eigenvectors  $\hat{\mathbf{r}}_{i-1/2}$  of  $\hat{\mathbf{A}}_{i-1/2}$  as its columns, and  $\hat{\Lambda}_{i-1/2}^+$  and  $\hat{\Lambda}_{i-1/2}^-$  are the diagonal matrices containing the positive and negative eigenvalues, respectively, of  $\hat{\mathbf{A}}_{i-1/2}$ . Further, for the method to be conservative, we must have that

$$\hat{\mathbf{A}}_{i-1/2} (\mathbf{Q}_i - \mathbf{Q}_{i-1}) = \sum_{p=1}^m s_{i-1/2}^p \mathcal{W}_{i-1/2}^p. \quad (48)$$

The approximate Riemann solution consists of  $m$  waves proportional to the eigenvectors  $\hat{\mathbf{r}}_{i-1/2}$  of  $\hat{\mathbf{A}}_{i-1/2}$ , propagating with speeds

$$s_{i-1/2}^p = \hat{\lambda}_{i-1/2}^p \quad (49)$$

given by the eigenvalues. The proportionality coefficients  $\beta_{i-1/2}^p$  can be found by solving the linear system

$$\mathbf{Q}_i - \mathbf{Q}_{i-1} = \sum_{p=1}^m \beta_{i-1/2}^p \hat{\mathbf{r}}_{i-1/2}^p, \quad (50)$$

and  $\beta_{i-1/2}^p$  can be interpreted as wave strengths (Toro, 1999, Section 2.3.3). The solution of the equation (50) is

$$\beta_{i-1/2} = \hat{\mathbf{R}}_{i-1/2}^{-1} (\mathbf{Q}_i - \mathbf{Q}_{i-1}), \quad (51)$$

whence the waves can be found as

$$\mathcal{W}_{i-1/2}^p = \beta_{i-1/2}^p \hat{\mathbf{r}}_{i-1/2}^p. \quad (52)$$

One disadvantage of using a linearized Riemann solver is that the approximate Riemann solution consists only of discontinuities, with no rarefaction waves (LeVeque, 2002, Section 15.3.5). This may require the use of an entropy fix. For the result presented here, no entropy fix is employed unless otherwise stated.

#### 4.2.2 Multifluid extension

The multifluid equations pose a problem, since they cannot be written in the conservation form (44). Nevertheless, a Roe-type method was derived by Tóuimi (1996) for the multifluid equations (including the energy equation), and a version for the isentropic multifluid equations was presented by Tóuimi and Kumbaro (1996). In those articles, the liquid density was assumed to be constant. Under the additional assumption of smooth solutions, the equation system could be written in conservation form, and a Roe matrix was derived, using some manipulations.

In the present work, we do not wish to make the above-mentioned assumptions. Hence we follow the approach of Evje and Flåtten (2003), who simply opted at showing that their candidate for a Roe matrix fulfilled the ‘weak’ conditions of Tóuimi and Kumbaro (1996). Here these conditions are given as stated by Evje and Flåtten (2003):

1.  $\hat{\mathbf{A}}_{i-1/2}$  is diagonalizable with real eigenvalues,
2.  $\hat{\mathbf{A}}_{i-1/2} \rightarrow \mathbf{A}(\bar{\mathbf{q}})$  smoothly as  $\mathbf{Q}_{i-1}, \mathbf{Q}_i \rightarrow \bar{\mathbf{q}}$ ,
3.  $\hat{\mathbf{A}}_{i-1/2} (\mathbf{Q}_i - \mathbf{Q}_{i-1}) = \Delta \mathbf{F}(\mathbf{Q}_{i-1}, \mathbf{Q}_i)$ .

The two first conditions are relatively straightforward. The last one involves some trickery. Herein,

$$\Delta F(\mathbf{Q}_{i-1}, \mathbf{Q}_i) = \begin{bmatrix} \{\alpha_g \rho_g u_g\} \\ \{\alpha_\ell \rho_\ell u_\ell\} \\ \{\alpha_g \rho_g u_g^2\} + \{\alpha_g \Delta p_{ig}\} + \bar{\alpha}_g \{p_g - \Delta p_{ig}\} \\ \{\alpha_\ell \rho_\ell u_\ell^2\} + \{\alpha_\ell \Delta p_{i\ell}\} + \bar{\alpha}_\ell \{p_\ell - \Delta p_{i\ell}\} \end{bmatrix}, \quad (53)$$

where

$$\{x\} = x_i - x_{i-1}. \quad (54)$$

The definition of  $\Delta F(\mathbf{Q}_{i-1}, \mathbf{Q}_i)$  is motivated by regrouping terms in the momentum equation (2) on page 3, to get

$$\frac{\partial}{\partial t}(\alpha_k \rho_k u_k) + \frac{\partial}{\partial x}(\alpha_k \rho_k u_k^2 + (p_k - p_{ik})\alpha_k) + \alpha_k \frac{\partial p_{ik}}{\partial x} = \alpha_k \rho_k g_x. \quad (55)$$

In the presence of discontinuities, the equations must be put in integral form in order for a solution to exist. In the momentum equation cast as above, the  $\alpha_k \partial p_{ik} / \partial x$  term poses problems, for the integral

$$\int_{\mathbf{q}_1}^{\mathbf{q}_2} \alpha_k \frac{\partial p_{ik}}{\partial \xi} d\xi \quad (56)$$

is dependent on the path  $\xi(\mathbf{q})$  between the two states  $\mathbf{q}_1$  and  $\mathbf{q}_2$ . Toumi and Kumbaro (1996) suggested writing such integrals as

$$\int_{\mathbf{q}_1}^{\mathbf{q}_2} \alpha_k \frac{\partial p_{ik}}{\partial \xi} d\xi = \bar{\alpha}_k(\alpha_{k,1}, \alpha_{k,2})(p_{ik,2} - p_{ik,1}), \quad (57)$$

defining the path  $\xi$  implicitly through the choice of an averaging function  $\bar{\alpha}_k(\alpha_{k,1}, \alpha_{k,2})$ . The expression derived by Toumi and Kumbaro (1996) was, somewhat inconveniently, not symmetric with respect to phasic indices. Evje and Flåtten (2003) proposed

$$\bar{\alpha}_k((\alpha_{k,1}, \alpha_{k,2})) = \frac{1}{2}((\alpha_{k,1} + \alpha_{k,2})) \quad (58)$$

instead, which is adopted here. Evje and Flåtten (2003) used an average state  $\hat{\mathbf{Q}}_{i-1/2}$  given by the following expressions, where the phasic indices have been dropped:

$$\begin{aligned} \hat{u} &= \frac{u_{i-1}\sqrt{(\alpha\rho)_{i-1}} + u_i\sqrt{(\alpha\rho)_i}}{\sqrt{(\alpha\rho)_{i-1}} + \sqrt{(\alpha\rho)_i}}, \\ \hat{\alpha} &= \frac{1}{2}(\alpha_{i-1} + \alpha_i), \\ \hat{\rho} &= \frac{1}{2}(\rho_{i-1} + \rho_i), \\ \widehat{\Delta p} &= \frac{1}{2}(\Delta p_{i-1} + \Delta p_i), \end{aligned} \quad (59)$$

where  $\Delta p$  is the interfacial pressure difference (27) on page 8. Putting all this into the coefficient matrix (25),  $\mathbf{A}(\hat{\mathbf{Q}}) = \hat{\mathbf{A}}(\mathbf{Q}_{i-1}, \mathbf{Q}_i)$ , using the equation of state (3) to remove the densities, and assuming that the phasic pressures are different only by a constant, one can confirm that condition 3 on page 13 is satisfied.

### 4.2.3 Considerations for the five-equation system

The verification of condition 3 on page 13 was performed for the four-equation system. However, the same exercise can be performed for the five-equation system, that is, the coefficient matrix (30). In doing that, it is necessary to define the average interfacial velocity. Here, similarly to what was done in the equation (58), we took

$$\bar{u}_{ik} = \frac{1}{2}(u_{ik,1} + u_{ik,2}), \quad (60)$$

and, in addition to equation (59), we set

$$\hat{u}_i = \frac{1}{2}(u_{i,i-1} + u_{i,i}). \quad (61)$$

Contrary to the case for the four-equation system, here the phasic pressures can be linearly independent.

Karni *et al.* (2004) presented results for a somewhat different Roe-type scheme for a seven-equation system, that is, including an energy equation for each phase.

## 5 Numerical tests

In this section, we analyse the Roe-type scheme for the four-equation system (Roe4), and for the five-equation system (Roe5) by performing numerical simulations.

For the numerical results presented here, simple boundary conditions were used. The variables not being set as boundary conditions, were extrapolated to the boundaries from the inner domain. A simple boundary treatment is sufficient for the present discussion, since it concentrates on the numerical scheme employed in the inner domain. More elaborate characteristic-based boundary conditions are discussed by Munkejord (2006), taking the water-faucet test case as an example.

### 5.1 Discontinuity moving in uniform flow

It is a basic test for numerical schemes that when no source terms are present, a flow with a uniform velocity and pressure should remain so, that is, variations should not be introduced in the velocities or in the pressure. This has sometimes been referred to as the principle of Abgrall (1996).

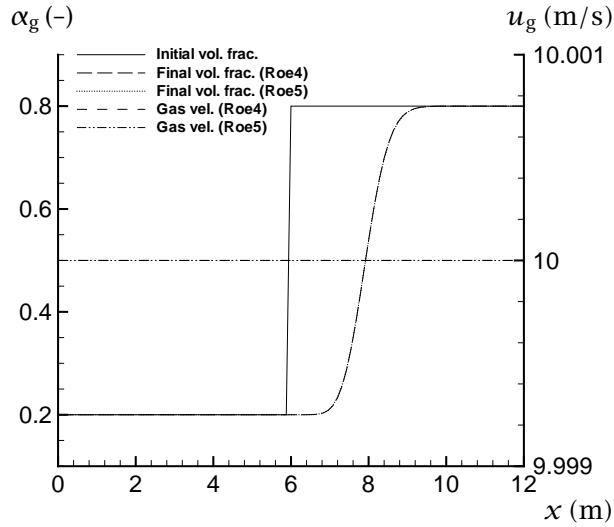


Figure 1: Discontinuity moving in uniform flow. First-order Roe4 and Roe5 schemes. Gas volume fraction (left abscissa) and gas velocity (right abscissa).

The agreement with Abgrall's principle was checked by performing a calculation in a 12 m long horizontal tube, where the velocities are initially equal to  $u_g = u_\ell = 10$  m/s and the pressure is  $p = 10 \cdot 10^5$  Pa. At the middle of the tube, the gas volume fraction jumps from 0.2 to 0.8. The results displayed in Figure 1 have been calculated with the first-order Roe4 and Roe5 schemes on a 101-point grid and using a CFL number of  $C = 0.9$ . Data are plotted at  $t = 0$  and at  $t = 0.2$  s. As can be seen, the volume-fraction discontinuity is advected to the right while being smeared. No disturbances are introduced in the gas velocity, and it remains constant. The same is true for the liquid velocity and the pressure (not shown). It can also be noted that the data produced by the Roe4 and the Roe5 schemes are identical to plotting accuracy. This is expected, since in the present case, the pressure is uniform and remains so, and hence the pressure relaxation should have nothing to say.

There is nevertheless a subtlety. When the CATHARE expression (22) is employed for the interfacial pressure difference, the coefficient matrix (25) for the four-equation system is non-diagonalizable for equal phasic velocities,  $u_g = u_\ell$ . Here this was overcome by employing the Soo model (20) with  $B_k = 1.0 - \varepsilon$ , where  $\varepsilon = 1 \cdot 10^{-10}$ . That is to say, a miniscule amount of numerical diffusion was introduced to render the coefficient matrix diagonalizable. While the effect of that is too small to be seen on the graph, it is observable when scrutinizing the numbers output by the numerical code in double precision.

For the Roe5 scheme, the above-mentioned measure was not necessary, and

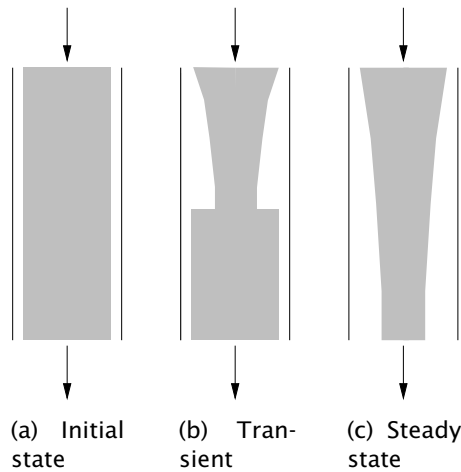


Figure 2: Sketch of the water-faucet test case. In the transient phase, a volume-fraction discontinuity propagates towards the exit.

the velocities and the pressure remained constant to full precision. A priori, this can be seen as an advantage for the Roe5 scheme compared to the Roe4 scheme, that is, the former is in some cases less sensitive to deficiencies in the model equations. However, as will be seen in the following, the price to pay is an increased numerical diffusion and a corresponding reduced accuracy for slow-moving waves.

## 5.2 Water-faucet test case

The water-faucet case is described in Ransom (1987), and it has become a common test case for one-dimensional two-fluid models.

### 5.2.1 Problem description

The problem consists of a vertical tube 12 m in length and 1 m in diameter. Here, of course, it is represented one-dimensionally. A schematic is shown in Figure 2. The top has a fixed volumetric inflow rate of water at a velocity of  $u_\ell^\circ = 10$  m/s, a liquid volume fraction of  $\alpha_\ell^\circ = 0.8$  and a temperature of  $T = 50$  °C. The bottom of the tube is open to the ambient pressure,  $p = 1.0 \cdot 10^5$  Pa, and the top of the tube is closed to vapour flow.

Initially, the flow is uniform throughout the computational domain, and the initial conditions are equal to the inlet conditions. A thinning of the liquid jet will take place due to the effect of gravity.

### 5.2.2 Analytical expressions for volume fraction and velocity

Ransom (1987) stated that when pressure variation in the vapour phase is ignored, the transient problem has a simple analytical solution. Coquel *et al.* (1997) provided the solution for the gas volume-fraction profile:

$$\alpha_g(x, t) = \begin{cases} 1 - \frac{\alpha_\ell^\circ u_\ell^\circ}{\sqrt{2gx + (u_\ell^\circ)^2}} & \text{if } x \leq u_\ell^\circ t + \frac{1}{2}gt^2, \\ 1 - \alpha_\ell^\circ & \text{otherwise,} \end{cases} \quad (62)$$

and the expression for the liquid velocity is given by Evje and Flåtten (2003):

$$u_\ell(x, t) = \begin{cases} \sqrt{(u_\ell^\circ)^2 + 2gx} & \text{if } x \leq u_\ell^\circ t + \frac{1}{2}gt^2, \\ u_\ell^\circ + gt & \text{otherwise.} \end{cases} \quad (63)$$

A partial description of the solution procedure can be found in Trapp and Riemke (1986).

### 5.2.3 Grid convergence and limiter functions

The grid convergence of the Roe4 method was tested on numerical grids ranging from 51 to 1601 grid points, using different limiter functions. The time step was set to  $\Delta t = 1.97 \cdot 10^{-5}$  s, which corresponds to a CFL number of  $C = 0.9$  for the finest grid.

First, liquid volume-fraction profiles are presented at time  $t = 0.6$  s in Figure 3 on the following page. In Figure 3(a), no limiter function was employed; this will be referred to as the first-order method. It is seen that the convergence was steady, but slow. In fact, the convergence was less than first order, even if the scheme is formally first-order accurate in space. This is due to the discontinuity in the solution. For discontinuous solutions, the smooth-solution order of the scheme can normally not be attained (see LeVeque, 2002, Section 8.7). In Figure 3(a), a data set is added for 3201 grid points to further illustrate the convergence. For this calculation, a CFL number of  $C = 0.9$  was used, that is, the time step was shorter than for the other grids.

Figure 3(b) shows the results for the monotonized central-difference (MC) limiter (van Leer, 1977; see also LeVeque, 2002, Section 6.11). It gave significantly better resolution than the first-order method, except for the coarse 51-point grid, where it gave overshoots. More details and calculations regarding limiter functions, and convergence order of the schemes, can be found in Munkejord (2005).

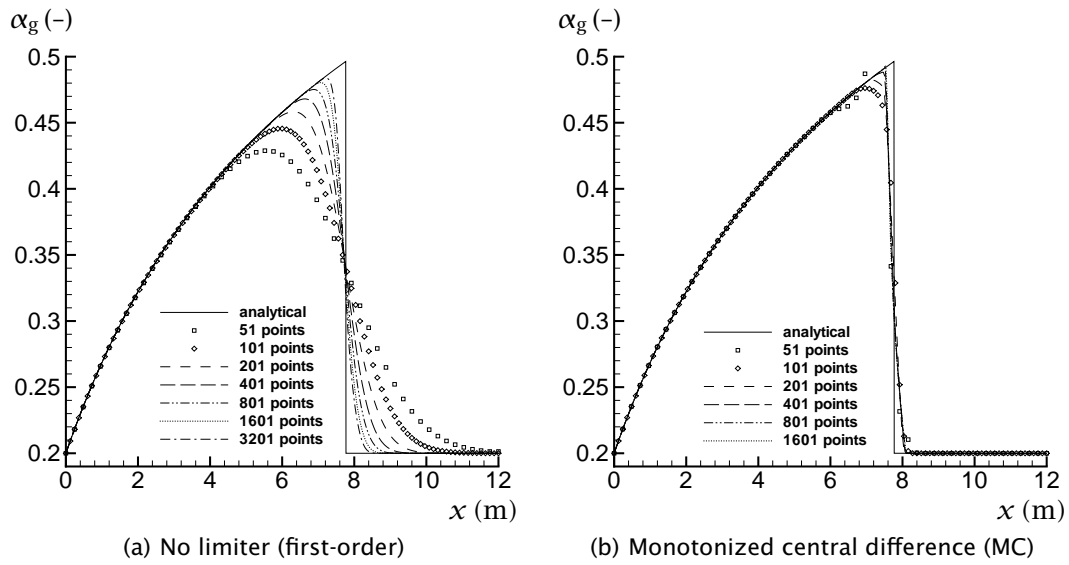


Figure 3: Gas volume fraction for the water faucet. Grid convergence of the Roe4 method with and without a limiter function.

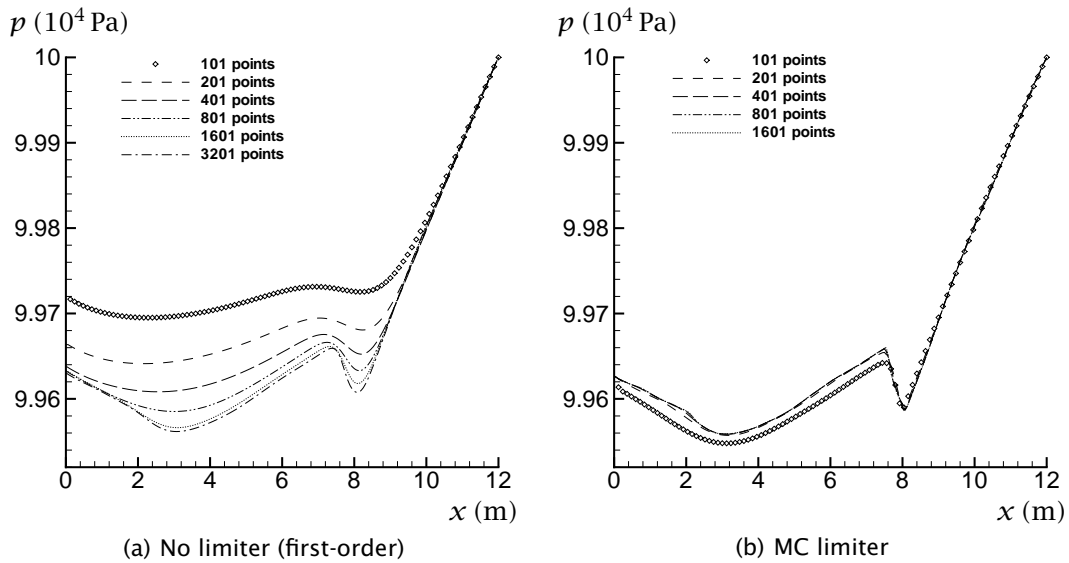


Figure 4: Pressure for the water faucet. Grid convergence of the Roe4 method with and without a limiter function.

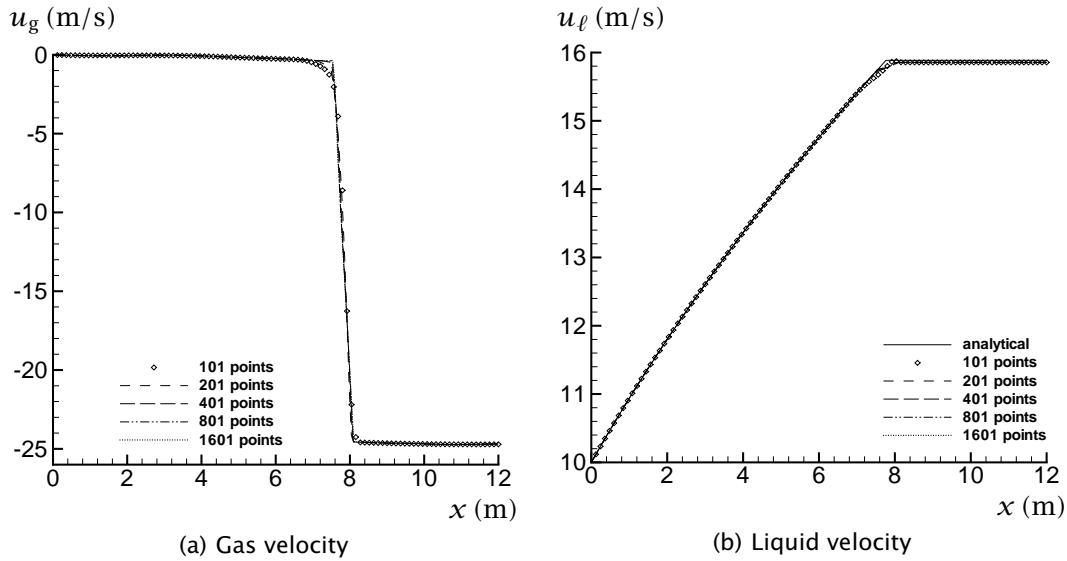


Figure 5: Velocities for the water faucet. Grid convergence of the Roe4 method.

**Pressure** The pressure is by far the most sensitive variable in the faucet case. It is shown in Figure 4 on the previous page for the MC limiter and for the first-order scheme. It can be observed that the first-order and the MC schemes seem to converge to the same value, and that the latter converges much faster. The pressure profile is also sensitive to the boundary treatment.

The remaining physical variables, namely the gas and liquid velocities, are displayed in Figure 5. As shown in Figure 5(b), the Roe4 method reproduced the analytical solution for the liquid velocity accurately, except just at the location of the volume-fraction discontinuity.

A comparison between the first-order scheme and the high-resolution method using the MC limiter function is given in Figure 6 on the next page. It is clear that the first-order method needs over ten times more grid points than the high-resolution method to produce a comparable volume-fraction profile.

Figure 7 on page 22 displays the results of computations performed using the Roe5 method with the MC limiter and numerical grids from 26 to 10001 points. The time-step length was the one corresponding to  $C = 0.9$  for the finest grid, in this case  $\Delta t = 1.06 \cdot 10^{-6}$  s. What is most striking about the figure, is that the results for the grids between 101 and 10001 points are virtually identical. This was not expected, and an explanation has yet to be found. Further, it can be seen that the Roe5 method is much more diffusive than the Roe4 method for the intermediate and fine grids. For the very coarse grid of 26 points, on the other hand, the Roe5 results are surprisingly good, and better than those of Roe4.

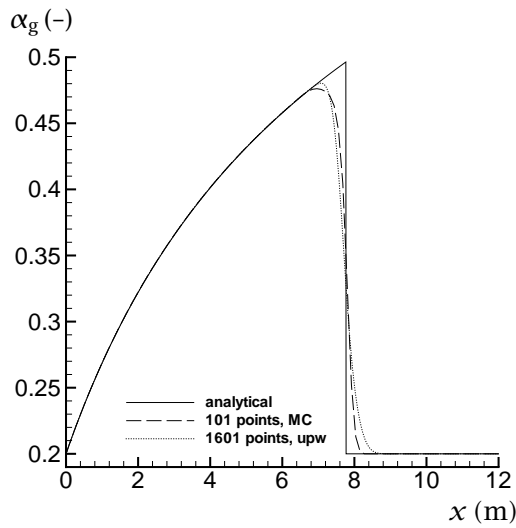


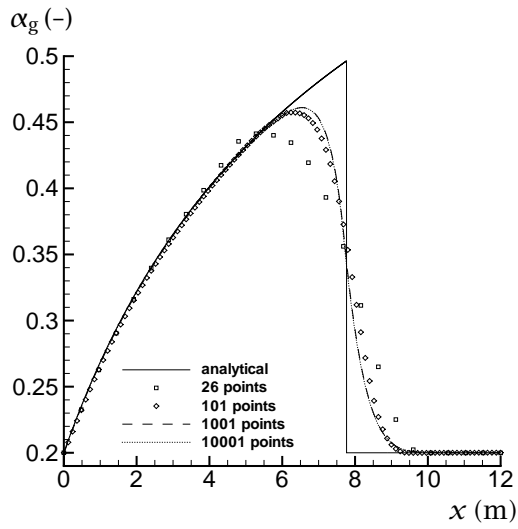
Figure 6: Gas volume fraction for the water faucet. Comparison of the first-order and the MC-limiter methods with the Roe4 scheme.

Reference is made to Munkejord and Papin (2007), where results obtained with the Roe5 scheme are shown to agree very well with those from a five-equation version of the discrete-equation method of Abgrall and Saurel (2003). Further, in Munkejord (2005, Chapter 4), the present test problems have been calculated using the first-order centred scheme (FORCE) of Toro (1999, Section 14.5.1).

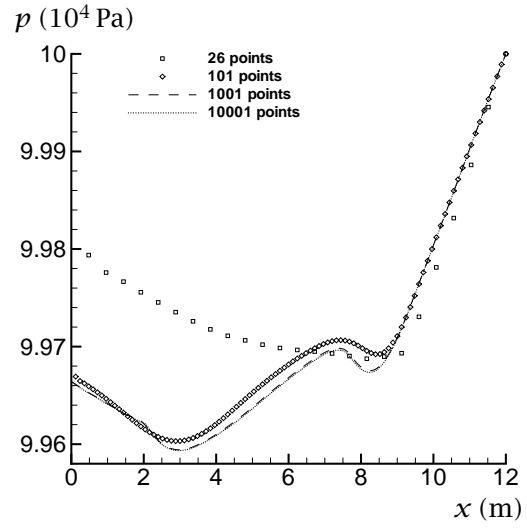
#### 5.2.4 Time-step convergence

The effect of time-step refinement, using the same 101-point grid and the MC limiter, is shown in Figure 8 on page 23. Regarding the Roe4 scheme in Figure 8(a), for CFL numbers below 0.5, the effect of time-step refinement is very slight.

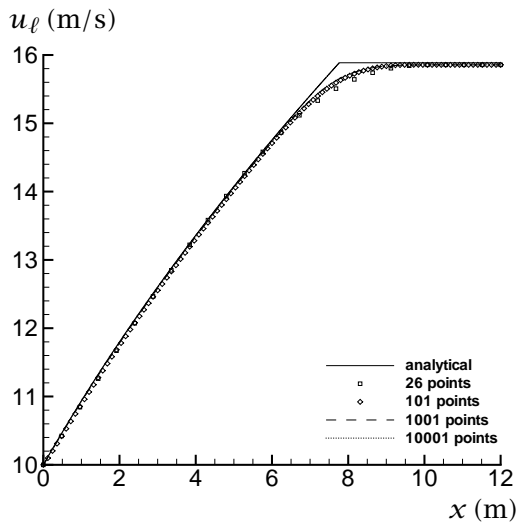
Results for the Roe5 scheme are given in Figure 8(b) for the case of no limiter (first-order), and in Figure 8(c) for the MC limiter. In the latter figure, the differences between the curves are striking compared to the miniscule ones for the Roe4 method in Figure 8(a). Furthermore, the difference between the first-order scheme and the MC-limiter scheme is very large. For the latter one, as can be seen in Figure 8(c), for  $C = 0.9$ , the volume-fraction profile is very smeared indeed. For  $C = 0.01$ , on the other hand, it lies between the profiles calculated using the MC-limited and first-order Roe4 method (Figure 3 on page 19). As the CFL number is reduced to miniscule values ( $C = 0.0001$ ), the curves seem to converge. Unfortunately, there is a slight overshoot to the left of the discontinuity.



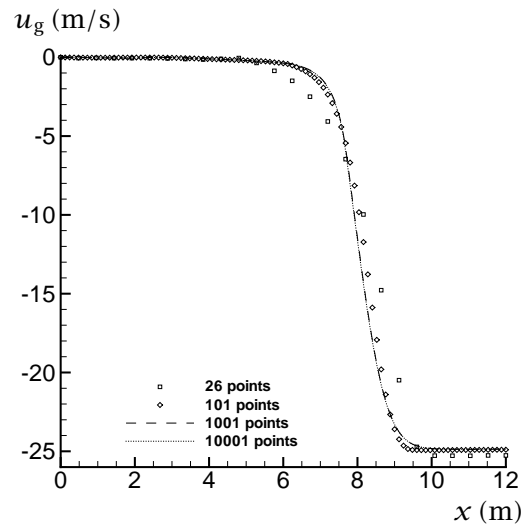
(a) Gas volume fraction



(b) Pressure

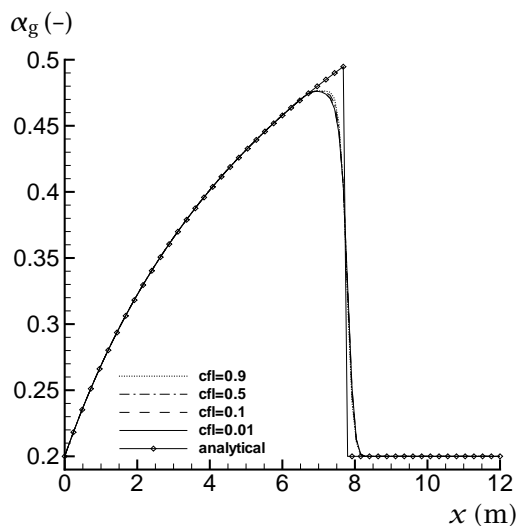


(c) Liquid velocity

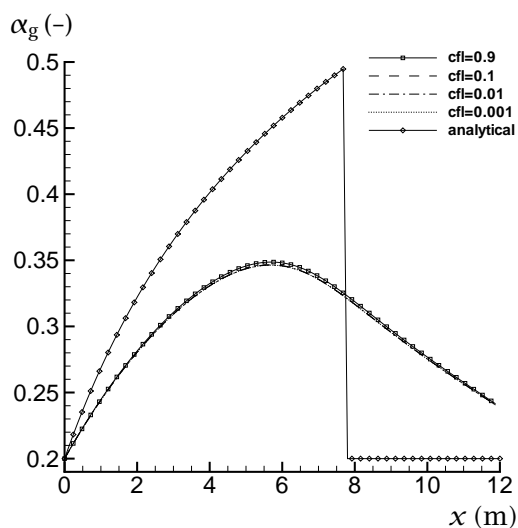


(d) Gas velocity

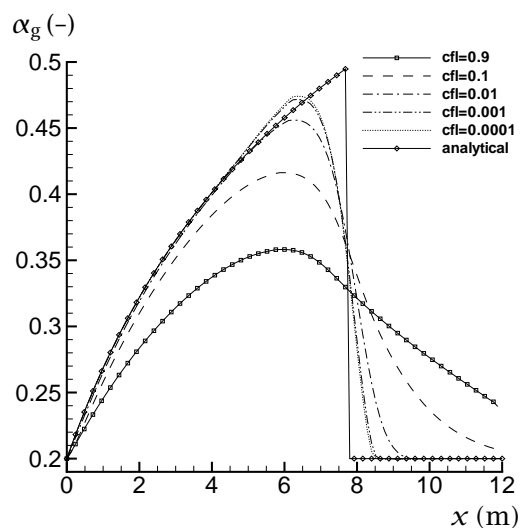
Figure 7: Water faucet. Grid refinement for the MC-limited Roe5 scheme.



(a) Roe4, MC-limiter



(b) Roe5, No limiter (first-order)



(c) Roe5, MC-limiter

Figure 8: Gas volume fraction for the water faucet. Effect of time-step length on the Roe4 and Roe5 schemes with and without MC-limiter.

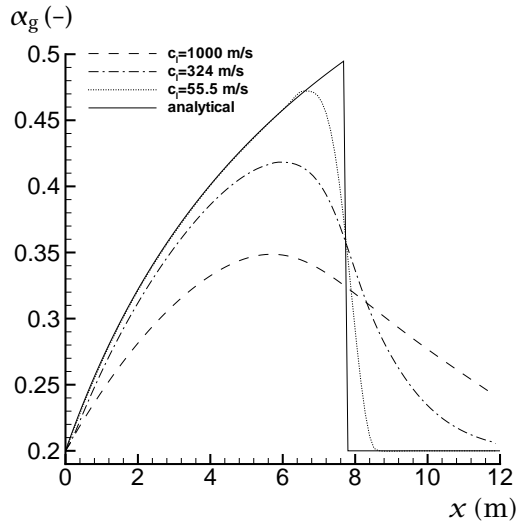


Figure 9: Gas volume fraction for the water faucet. Effect of liquid speed of sound on the Roe5 scheme.

### 5.2.5 Effect of liquid speed of sound

The Roe5 scheme is rather diffusive, and it is tempting to try to remove some of the diffusion. One way of doing that, is by reducing the liquid speed of sound. While this changes the problem under consideration, it illustrates the behaviour of the scheme. An investigation of the effect of the speed of sound is shown in Figure 9. The calculations have been performed on a grid of 101 points, using the MC limiter and the same time-step length of  $\Delta t = 1.06 \cdot 10^{-4}$  s, corresponding to  $C = 0.9$  for the case of the highest (that is, closest-to-physical) liquid speed of sound. The only thing being varied, is the liquid speed of sound,  $c_\ell$ , together with a corresponding variation of  $\rho_\ell^\circ$  to maintain the same initial liquid density,  $\rho_\ell = 1000 \text{ kg/m}^3$ .

First, we tried to obtain the same maximum eigenvalue as for the four-equation system. At  $t = 0.6$  s, the four-equation system has  $\lambda_{\max} \approx 340$  m/s, and the maximum liquid speed is about 16 m/s. Hence the liquid speed of sound was set to  $c_\ell = 324$  m/s. The figure shows that this gave less diffusion, but it is still far from what one obtains using the Roe4 scheme.

Next, as an educated guess,  $c_\ell = 55.5$  m/s was tried. This helped considerably on the volume-fraction profile, which is now better than the one produced with the first-order Roe4 method on the same grid (see Figure 3(a) on page 19). Still, it does not reach the volume-fraction profile from the MC-limited Roe4 method (Figure 3(b)).

We remark that the phasic speeds of sound have an effect on the Roe4 scheme

as well, but to a much lesser extent than on the Roe5 scheme. This is thought to be due to the pressure-relaxation being performed in the latter scheme. Indeed, in the pressure-relaxation procedure, the densities (and hence pressures) are tightly linked to the volume fraction. Hence fast-moving pressure waves are transferred to the volume fraction, and this may be an explanation of the smeared volume-fraction profiles of the Roe5 scheme.

It is possible that the diffusion introduced by the pressure relaxation may be reduced by the use of a low-Mach-number method. To analyse this is left for future work.

### 5.2.6 Wave propagation speed

The different eigenvalues for the four-equation system and the five-equation system might lead one into thinking that sonic waves in the two systems would propagate at different speeds (for instance Flåtten, 2003, Section 3.3.1); for the faucet case at  $t = 0.6$  s, the maximum eigenvalue in the four-equation system is about 340 m/s, while it is 1013 m/s in the five-equation system.

However, the above simple consideration does not take the instantaneous pressure-relaxation procedure into account. To illustrate this, we study the following example calculation: In the faucet case, a wave forms at the inlet at  $t = 0$ , and it travels towards the outlet. This is shown in Figure 10 on the next page. Calculations have been performed using the Roe4 and Roe5 schemes, on a grid of 101 points. Both schemes were run using about  $C = 0.2$  (that is, a shorter time-step for the Roe5 scheme) and the MC limiter. Figure 10(a) shows snapshots of  $(\alpha\rho u)_g$  at  $\Delta t = 0.005$  s intervals, while the time history of the same variable at  $x = 12$  m is shown in Figure 10(b).

Figure 10(a) clearly shows that the disturbance propagates with the same velocity in the two schemes. Moreover, no faster-moving disturbances could be observed in any of the variables in the Roe5 scheme.

As can be seen from Figure 10(b), the wave reached the boundary at about  $t = 0.037$  s. At this time, there was virtually no difference between the Roe4 and the Roe5 schemes.

The wave propagation speed was found to be  $12 \text{ m}/0.037 \text{ s} \approx 324 \text{ m/s}$ , whereas the maximum eigenvalue of the coefficient matrix of the four-equation system was 317 m/s at  $t = 0.005$  s, increasing to 324 m/s at  $t = 0.2$  s. The correspondence is clear.

As can be seen for instance in Figure 10(b),  $(\alpha\rho u)_g$  immediately starts to increase. The reason for this, is the action of gravity.

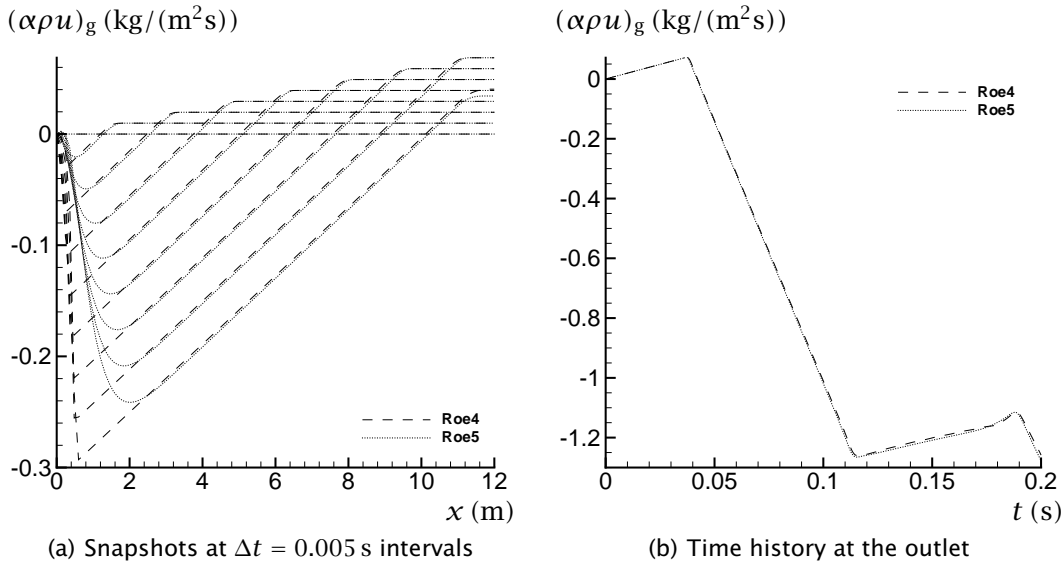


Figure 10: Gas volumetric momentum for the water faucet. Comparison of wave propagation in the Roe4 and the Roe5 schemes.

### 5.2.7 Non-hyperbolic underlying model

One of the advantages of the Roe5 method perceived in Section 3.2 on page 8, is that the coefficient matrix remains hyperbolic, even when the ‘0 model’

$$\Delta p_{ik} = 0 \quad (64)$$

is taken for the interfacial pressure difference. For such cases, the ‘underlying’ four-equation model is non-hyperbolic with complex eigenvalues.

Figure 11 on the next page shows the water-faucet gas volume-fraction profile calculated on a grid of 101 points using the MC limiter and a quite short time-step length of  $\Delta t = 1.06 \cdot 10^{-6}$  s. Two models have been employed for the interfacial pressure difference; the CATHARE model (22) and the 0 model (64). Further, two different liquid speeds of sound were tried;  $c_\ell = 1000$  m/s and  $c_\ell = 55.5$  m/s, as commented upon in Section 5.2.5 on page 24.

As can be observed, the use of the 0 model for the interfacial pressure difference together with the low liquid speed of sound results in a severe undershoot in front of the discontinuity, whereas the curve for the CATHARE model and the low liquid speed of sound is quite well-behaved. This may indicate that the use of Roe5 scheme and similar methods provides no easy way to avoid the problem of complex eigenvalues in the four-equation model.

For the high liquid speed of sound, no anomalies were incurred by the 0 model. This might be a result of the high liquid speed of sound providing ‘enough’

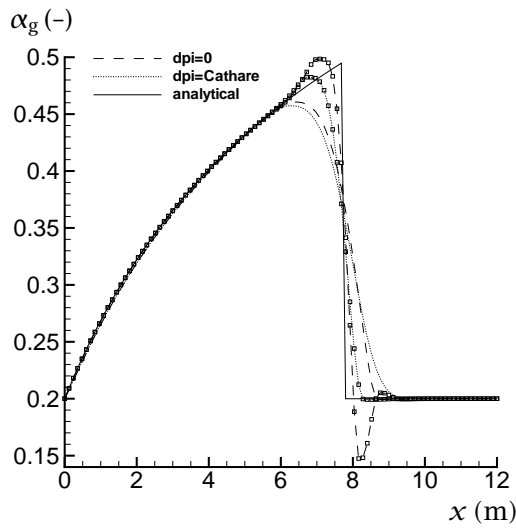


Figure 11: Gas volume fraction for the water faucet. Roe5 scheme. Results for the 0 model and the CATHARE model for the interfacial pressure difference, for two liquid speeds of sound,  $c_\ell = 1000$  m/s and  $c_\ell = 55.5$  m/s (with  $\square$ ).

diffusion in the Roe5 scheme. Indeed, this was the case even on a fine grid of 20001 points.

Karni *et al.* (2004) reported undershoots for their Roe-type solver with pressure relaxation and the 0 model for the interfacial pressure difference, even for equation-of-state parameters giving a high liquid speed of sound, speculating that this might be due to the ill-posedness of the underlying one-pressure two-phase model. A similar effect was also observed by Munkejord (2005, Chapter 4) for the first-order centred scheme FORCE.

### 5.3 Large relative velocity shock tube

The large relative velocity (LRV) shock was investigated by Cortes *et al.* (1998); Evje and Flåtten (2003). The initial left and right states are given in Table 2 on the next page. The result of grid refinement for the Roe4 scheme is shown in Figure 12 on the following page for the primitive variables at  $t = 0.1$  s. The calculations were run with a time-step length of  $\Delta t = 2.35 \cdot 10^{-5}$  s, corresponding to  $C = 0.9$  for the finest grid, and the MC limiter was used.

As Evje and Flåtten (2003) pointed out, the wedge that can be seen in the volume fraction, and also in the gas velocity, at  $x = 50$  m, is two volume-fraction waves. This detail is shown for the volume fraction in Figure 13. In the figure, data have been added for a grid of 40001 points and  $C = 0.9$ , something which

Table 2: Initial conditions in the large relative velocity (LRV) shock tube

Quantity	symbol (unit)	left	right
Gas volume fraction	$\alpha_g$ (-)	0.29	0.30
Pressure	$p$ (kPa)	265	265
Gas velocity	$u_g$ (m/s)	65	50
Liquid velocity	$u_\ell$ (m/s)	1	1

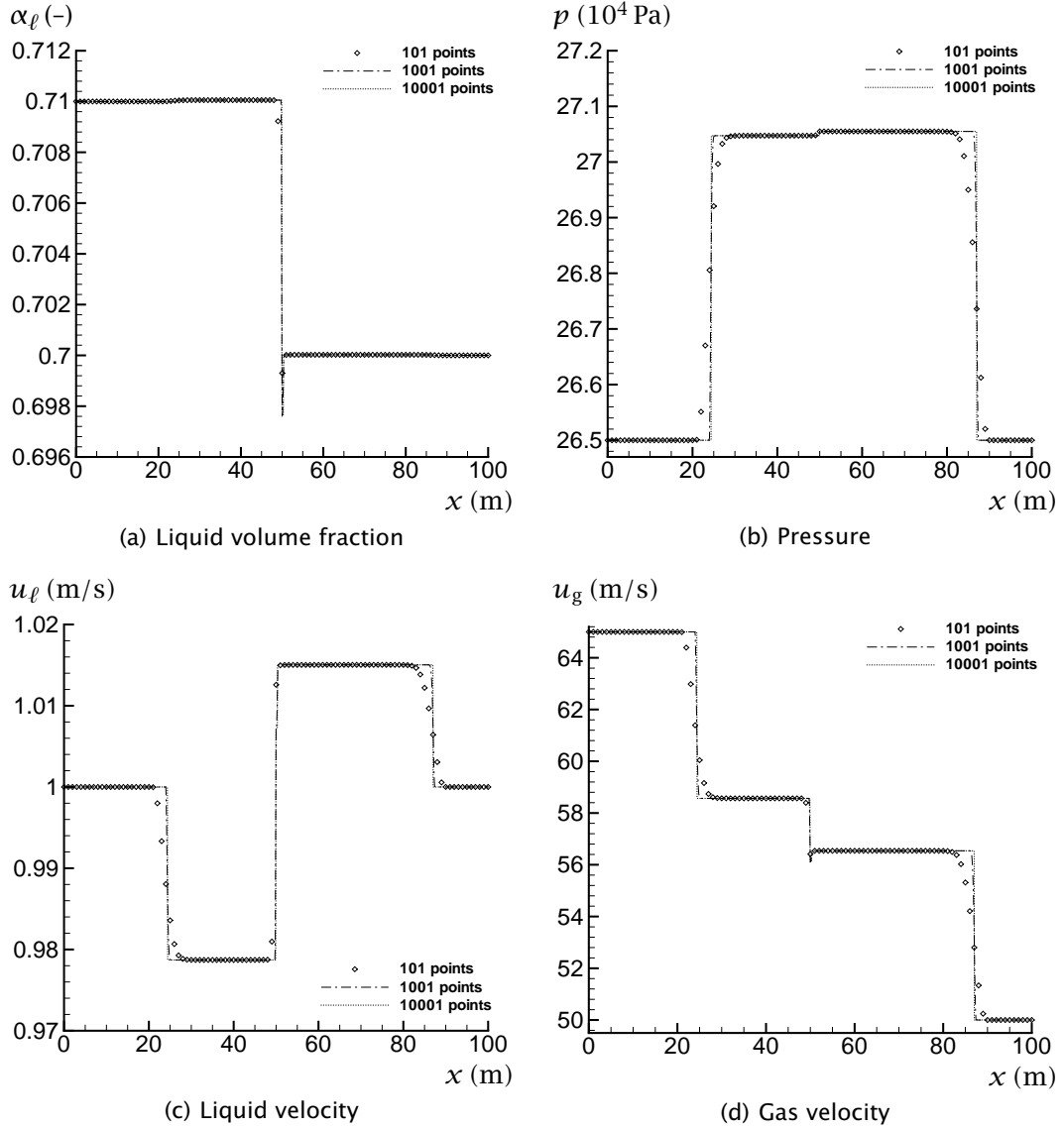


Figure 12: LRV shock tube. Grid refinement for the Roe4 (MC) scheme.

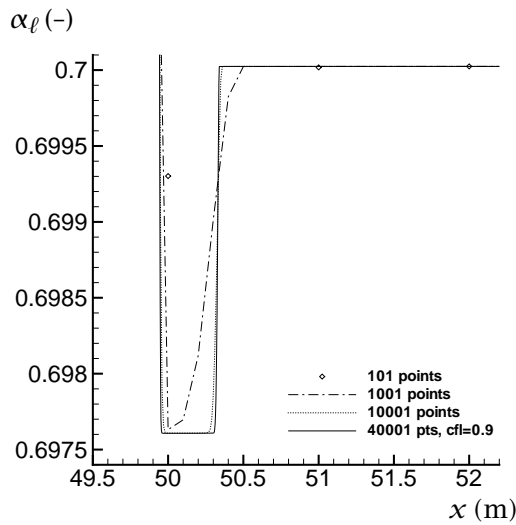


Figure 13: LRV shock tube. Close-up of volume-fraction waves for the Roe4 scheme.

clearly shows the convergence; both the fine-grid solutions are practically equal, and they are also thought to be practically equal to the true solution to the equation system.

The resolution of sonic waves is dependent on the CFL number. Time-step refinement is shown in Figure 14 on the next page for a grid of 101 points. As can be seen, the resolution of the sonic waves (at about  $x = 25$  m and  $x = 85$  m) improves with increasing CFL number, whereas the resolution of volume-fraction waves (at  $x = 50$  m) is largely unaffected. The latter effect was also seen for the faucet case in the previous subsection. An improving sonic-wave resolution with increasing CFL number is in accordance with what is known about upwind methods. For instance, an upwind method can solve the advection equation exactly for  $C = 1$ .

The effect of the limiter function is displayed in Figure 15 on the following page. It can be observed that employing the MC limiter function gives a significantly improved resolution of both the sonic waves (Figure 15(a)) and the volume-fraction waves (Figure 15(b)). Still, the effect in the present case is perhaps less striking than what was observed for the faucet case in Figure 3 on page 19. The calculation of Figure 15(b) has been performed on a fine grid, since the volume-fraction wedge is confined to a small area.

Figure 16 on page 31 shows the result of grid refinement for the Roe5 scheme using the MC limiter. The time-step length was  $\Delta t = 8.99 \cdot 10^{-6}$  s, corresponding to  $C = 0.9$  on the finest grid of 10001 points. The results obtained with the Roe4 method on the fine grid are drawn as a reference. The figure shows that

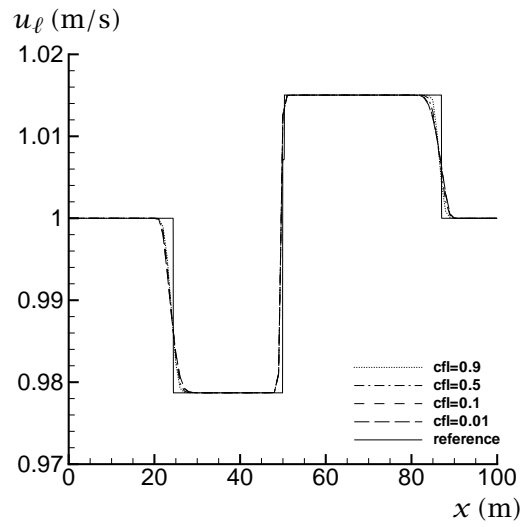


Figure 14: Liquid velocity for the LRV shock tube. Time-step refinement for the Roe4 (MC) scheme on a grid of 101 points. The reference solution is calculated on a 10001-point grid.

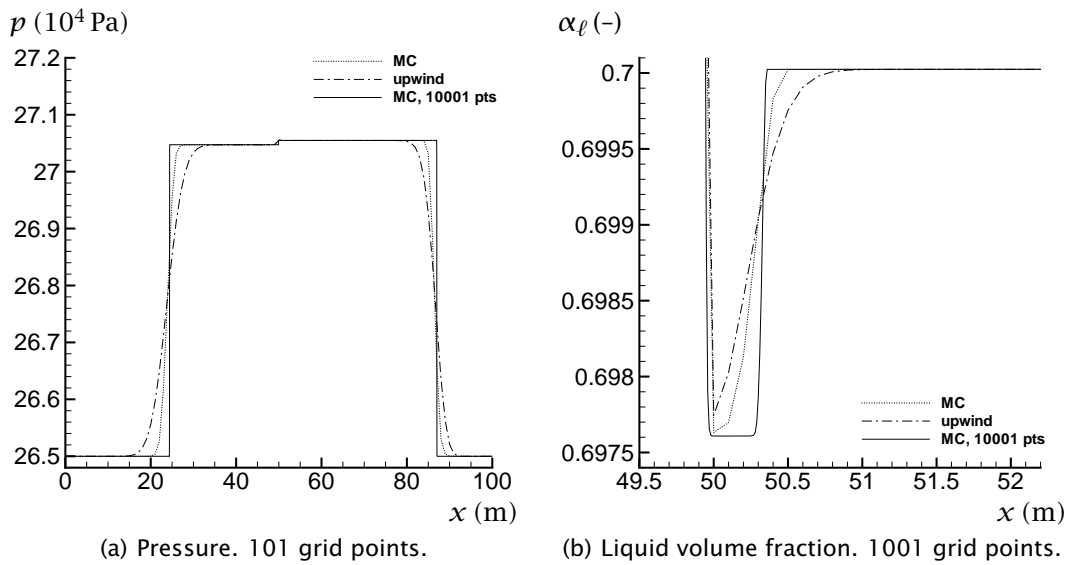


Figure 15: LRV shock tube. Effect of limiter function for the Roe4 scheme, with fine-grid data as reference.  $C = 0.9$ .

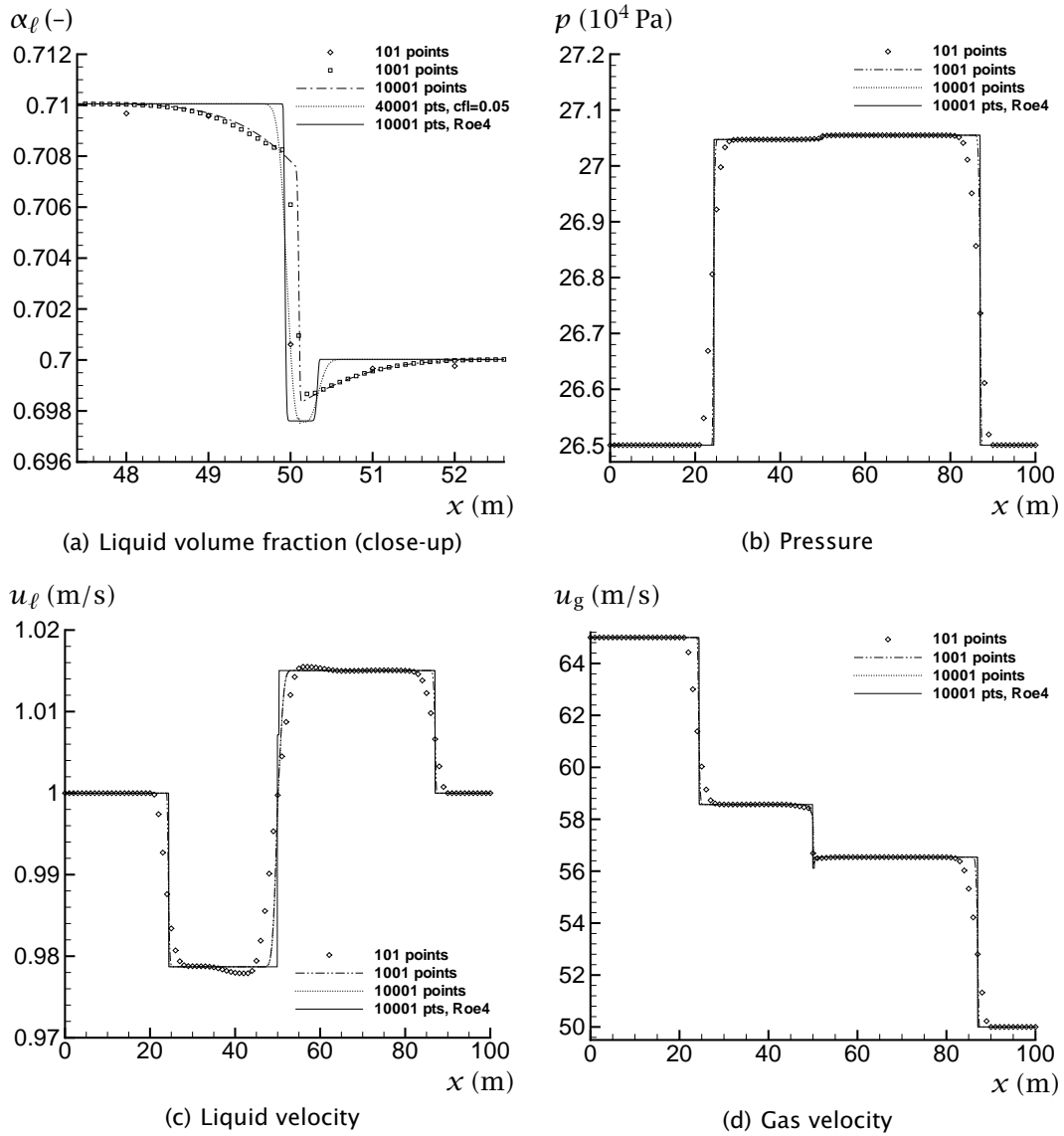


Figure 16: LRV shock tube. Grid refinement for the Roe5 (MC) scheme.

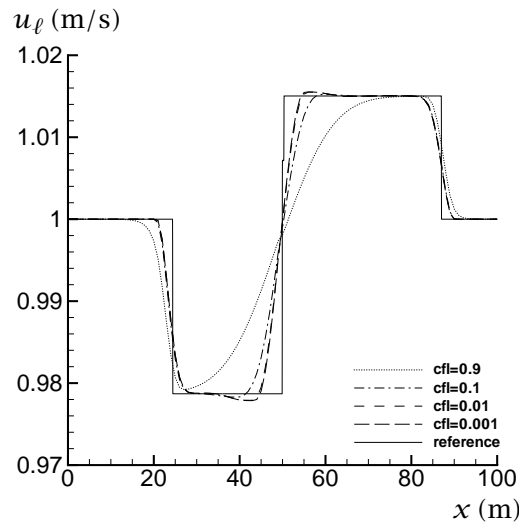


Figure 17: Liquid velocity for the LRV shock tube. Time-step refinement for the Roe5 (MC) scheme on a grid of 101 points. The reference solution is calculated using the Roe4 (MC) scheme on a 10001-point grid.

the results of the Roe5 scheme converge towards those of the Roe4 scheme. However, for the volume fraction wave at  $x = 50$  m, the convergence is very slow. This is thought to be mainly due to the high diffusivity of the Roe5 scheme, and it can be seen in Figure 16(a) for the liquid volume fraction, where the focus is on the middle of the shock tube. In that figure, results from the Roe5 method on a very fine grid of 40001 points, using  $C = 0.05$ , have been added to illustrate the effect of further grid and time-step refinement. In addition to slow convergence, the Roe5 method suffers from instabilities at the left-hand-side of the volume-fraction wedge.

Time-step refinement is displayed in Figure 17 for a grid of 101 points. Similarly to what was seen for the Roe4 method, the sonic waves are slightly better resolved for the highest CFL number. Contrary to the Roe4 method, however, the resolution of the liquid velocity at the discontinuity at  $x = 50$  m is strongly time-step dependent. Here, the resolution is increasingly poor for increasing CFL numbers.

#### 5.4 Toumi's shock tube

The present problem was introduced as a test case by Toumi (1996) for his Roe-type solver for a six-equation model. It has also been studied by Tiselj and Petelin (1997); Paillère *et al.* (2003) and Evje and Flåtten (2005), the latter researchers using a four-equation model. The initial values are given in Table 3,

Table 3: Initial conditions in Toumi’s shock tube

Quantity	symbol (unit)	left	right
Gas volume fraction	$\alpha_g$ (-)	0.25	0.10
Pressure	$p$ (MPa)	20	10
Gas velocity	$u_g$ (m/s)	0	0
Liquid velocity	$u_\ell$ (m/s)	0	0

and no source terms are considered.

Unfortunately, with the CATHARE expression (22) for the interfacial pressure difference, the coefficient matrix (25) of the four-equation system is not diagonalizable for the initial condition  $u_g = u_\ell$ . Hence, an ad hoc approach was taken, combining the CATHARE and the Soo models:

$$p_k - p_{ik} = \Delta p_{ik} = \gamma \frac{\alpha_g \alpha_\ell \rho_g \rho_\ell}{\alpha_g \rho_\ell + \alpha_\ell \rho_g} (u_g - u_\ell)^2 + (1 - B_k) p_k, \quad (65)$$

where the displacement factor was set to a high value;  $B_k = 0.999999$ , that is, giving negligible additional diffusion, but making the coefficient matrix diagonalizable.

For Toumi’s shock tube, the ‘plain’ Roe4 scheme converges to physically implausible results with an extra wave. In the present calculations, this was remedied by employing the entropy fix of Harten (1983) (see also e.g. LeVeque, 2002, Section 15.3.5).

The result of grid refinement for the Roe4 scheme using the MC limiter is shown in Figure 18 on the following page. The time-step length was  $\Delta t = 9.13 \cdot 10^{-6}$  s, which corresponds to  $C = 0.5$  for the finest grid.

A comparison of the first-order Roe4 scheme employing Harten’s entropy fix, and the first-order Roe5 scheme is shown in Figure 19 on page 35. The grid size was 10001 points, and the CFL number was  $C = 0.9$ . No limiter was employed in this case, since for the Roe5 scheme, the MC limiter introduced instabilities at the middle of the tube. On the other hand, the Roe5 scheme needed no additional diffusion in the form of an entropy fix or the use of the combined interfacial pressure-difference model (65). For the temporal and spatial resolutions investigated, the results were different in the middle section of the shock tube, between about  $x = 50$  m and  $x = 60$  m. For the Roe5 scheme, the volume fraction and the velocities in this section all had gradients, whereas the Roe4 scheme produced plateaux. The latter behaviour corresponds to those of other methods (Evje and Flåtten, 2005). Furthermore, the discontinuity at  $x = 60$  m is more sharply resolved by the Roe4 scheme.

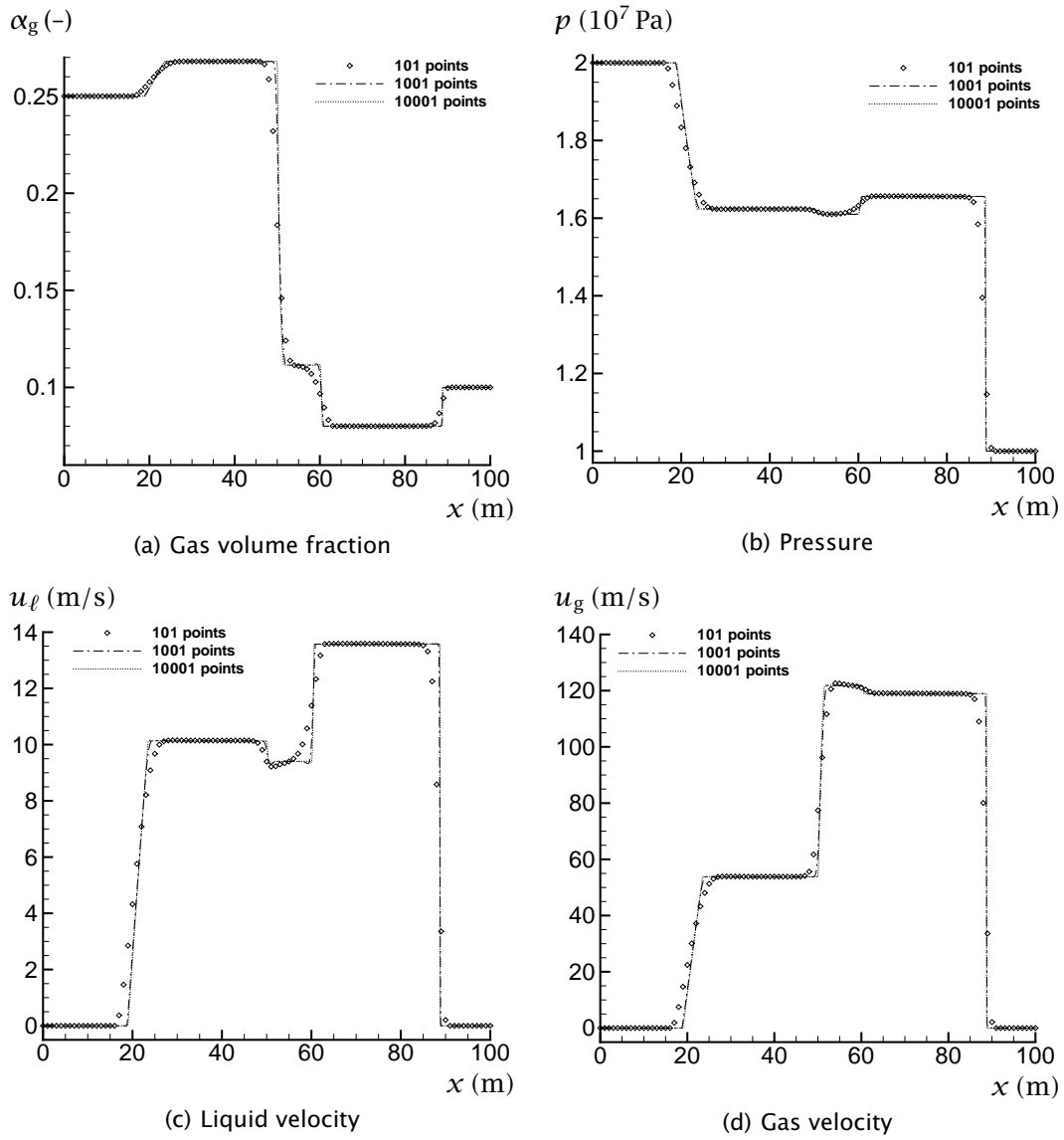


Figure 18: Toumi's shock tube. Grid refinement for the Roe4 (MC) scheme employing Harten's entropy fix.

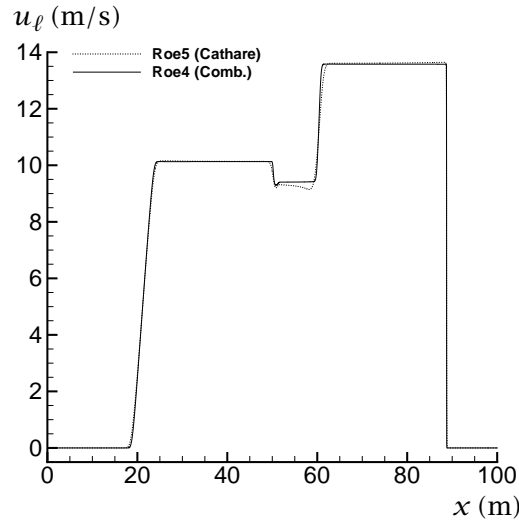


Figure 19: Liquid velocity for Toumi’s shock tube. Comparison of the first-order Roe4 (with entropy fix) and Roe5 schemes on a grid of 10001 points.

## 5.5 Effect of the pressure-relaxation parameter

In the preceding subsections, instantaneous pressure relaxation was always used in the Roe5 method. Now we will investigate the effect of varying the pressure-relaxation parameter,  $r_p$ , in the equation (9).

### 5.5.1 Water-faucet case

Consider Figure 20 on the following page, showing the gas volume fraction for the water-faucet case. The calculations have been performed using a 101-point grid, the MC limiter and a time-step length of  $\Delta t = 1.06 \cdot 10^{-6}$  s. The curve labelled ‘instant’ has been calculated with instantaneous pressure relaxation, and it is equal to that already shown in Figure 7(a). The other curves have been calculated using the fractional-step method outlined in Section 2.2.2 for a finite pressure-relaxation coefficient. The analytical solution of Section 5.2.2 has been added for reference. The effect of the pressure-relaxation parameter,  $r_p$ , is clearly seen in the figure: The smaller the  $r_p$ , the flatter the volume-fraction profile becomes. For  $r_p = 0$ , the volume-fraction remains constant. This can be understood by considering the volume-fraction evolution equation (9). Initially,  $\partial \alpha_g / \partial x = 0$ , and since  $r_p = 0$ ,  $\partial \alpha_g / \partial t = 0$ , which means that the volume fraction does not change.

It should also be noted that the transition between instantaneous and finite-rate pressure relaxation is smooth.

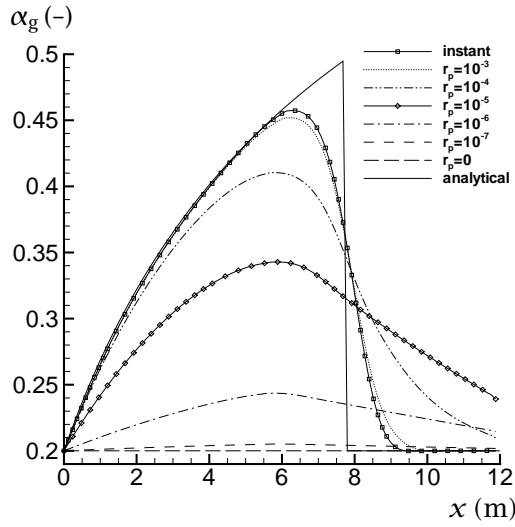


Figure 20: Gas volume fraction for the water faucet. Effect of pressure-relaxation parameter  $r_p$  on the Roe5 (MC) scheme for a grid of 101 points.

### 5.5.2 Toumi's shock tube

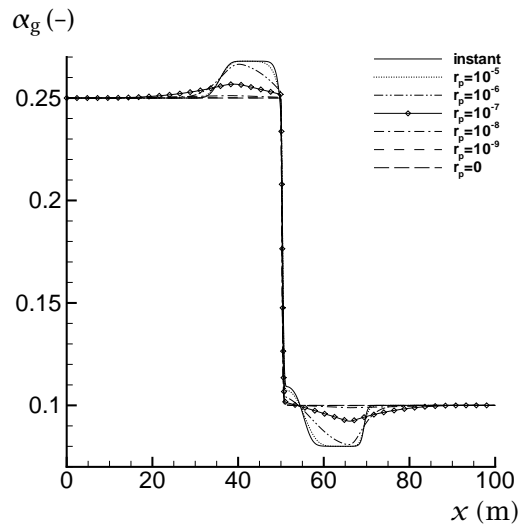
A further example of the effect of the pressure-relaxation parameter is shown in Figure 21 on the next page. Here, Toumi's shock tube has been calculated on a grid of 1001 points using no limiter and a time-step length of  $\Delta t = 8.87 \cdot 10^{-6}$  s. However, as opposed to the case of the one-pressure calculations, here, the results are shown at  $t = 0.04$  s. This has been done to avoid interaction with the boundaries.

Figure 21(b) shows an interesting plot of the liquid velocity. For a low value of the pressure-relaxation parameter,  $r_p$ , the two sonic waves can be seen to have reached about  $x = 10$  m and  $x = 90$  m. As  $r_p$  is increased, those two fast sonic waves are gradually suppressed, and the effect of the gas phase becomes more and more visible.

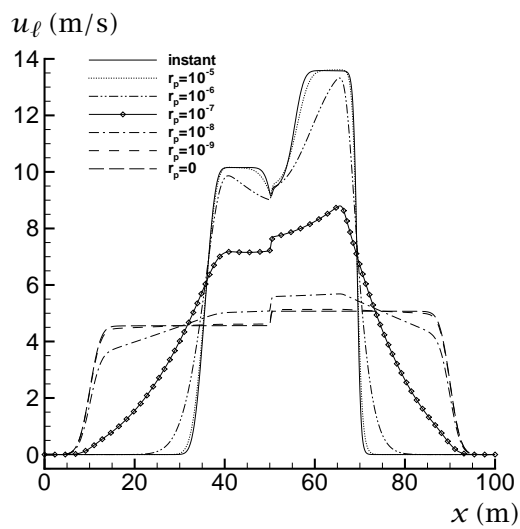
The approximate speed of the sonic waves can be read from the figure. For a low  $r_p$ , the average speed of the right-going wave is  $40 \text{ m} / 0.04 \text{ s} = 1000 \text{ m/s}$ , which closely corresponds to the eigenvalue  $u_\ell + c_\ell$ . As the pressure-relaxation coefficient is increased, the sonic speed is reduced to that of the four-equation model, as was seen for instance in Figure 19 on the preceding page.

The discontinuity at the middle of the tube moves to the right with a speed corresponding to the interfacial velocity,  $u_i$ , (see (8)), which is practically equal to the liquid velocity.

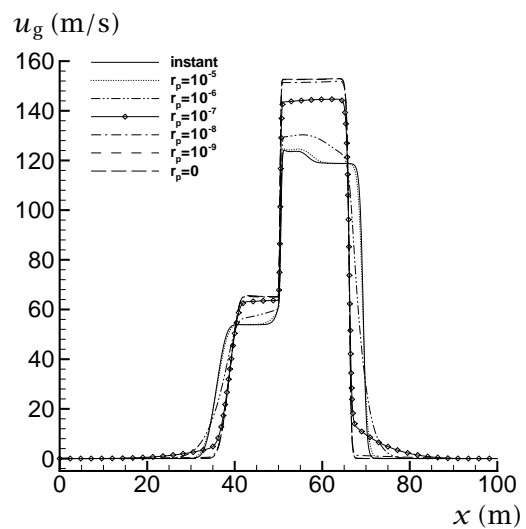
The gas and liquid pressures are displayed in Figures 21(d) and 21(e), and it can be observed how the two independent pressures converge to one as  $r_p$  is



(a) Gas volume fraction



(b) Liquid velocity



(c) Gas velocity

Figure 21: Toumi's shock tube at  $t = 0.04$  s. Effect of the pressure-relaxation parameter  $r_p$  in the Roe5 (first-order) method for a grid of 1001 points.

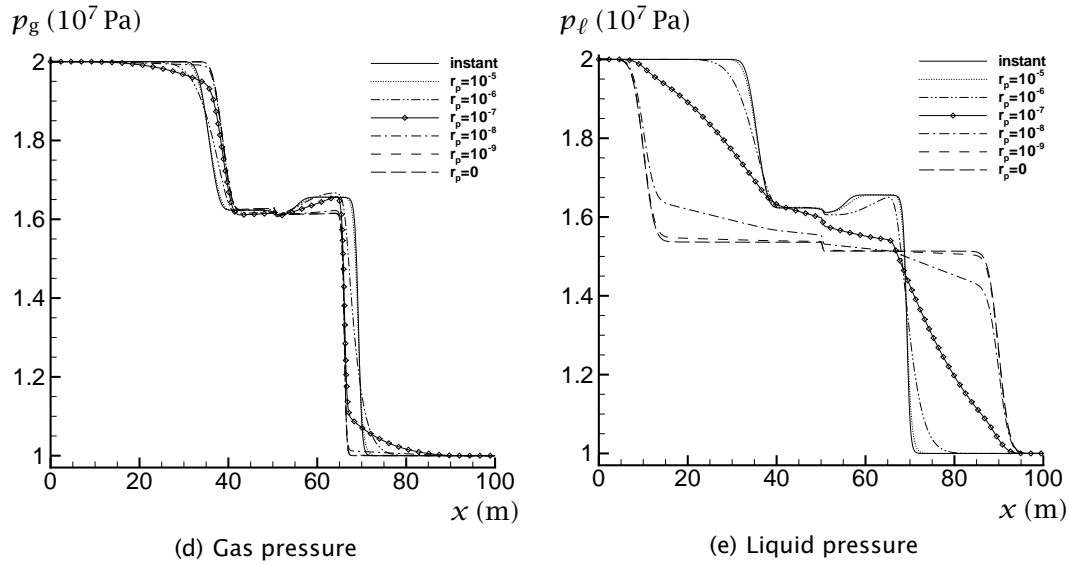


Figure 21: (Continued) Toumi's shock tube at  $t = 0.04$  s. Effect of the pressure-relaxation parameter  $r_p$  in the Roe5 (first-order) method for a grid of 1001 points.

increased.

## 5.6 Summary

A Roe-type scheme for the four-equation system (Roe4) has been tested on various cases from the literature. In the present work, the high-resolution approach of LeVeque (2002) has been successfully applied to the multifluid equations. For discontinuity problems such as the water-faucet case, a significant improvement was achieved compared to the conventional first-order Roe scheme.

In the large relative velocity (LRV) shock-tube problem, the effect of the high-resolution correction was less pronounced than for the faucet case. The resolution of sonic waves was seen to be time-step dependent.

A Roe-type scheme for the five-equation system has been derived (Sections 3 and 4): The two-velocity, two-pressure two-fluid model is first advanced in time, then a pressure-relaxation procedure is performed, yielding the same pressure in the two phases. The resulting scheme, Roe5, has been tested and compared to Roe4.

The Roe5 scheme was found to be significantly more diffusive than the Roe4 scheme, particularly for slow waves. The diffusion is a strong function of the chosen time-step length, the grid size, whether a limiter function is employed or

not, and also the liquid speed of sound.

Interestingly, for the faucet case, the MC-limited Roe5 scheme performed better than the Roe4 scheme for the very coarse grid of 26 points.

For fine grids and short time steps, the Roe5 scheme mostly converges to the same results as the Roe4 scheme. The differences seen are thought to be mainly due to the high diffusivity of the Roe5 scheme.

It was found that the sonic wave-propagation speed is the same in the Roe4 and the Roe5 schemes.

For Toumi's shock tube, it was required to use an entropy fix with the Roe4 scheme. For the Roe5 scheme, on the other hand, no fix was necessary, but the produced results were slightly less plausible.

The coefficient matrix employed in the Roe5 scheme is diagonalizable with real eigenvalues even in the case of zero interfacial pressure difference. This is a main difference between the Roe5 and the Roe4 schemes. Even so, oscillations normally associated with complex eigenvalues were produced for a low liquid speed of sound in the water-faucet test case. This may indicate that the Roe5 scheme and similar methods provide no easy remedy against complex eigenvalues in the two-fluid model.

The effect of finite-rate pressure relaxation in the Roe5 method was tested. As the pressure-relaxation parameter was increased, the solution gradually approached that obtained using instantaneous pressure relaxation.

The good correspondence between the results obtained using the Roe4 scheme and those of the Roe5 scheme with instantaneous pressure relaxation, indicates that the latter may be regarded as a numerical method to solve the four-equation system.

## 6 Conclusions

- The Roe5 scheme with instantaneous pressure relaxation can be regarded as a numerical method to solve the four-equation system. It is significantly more diffusive than the Roe4 scheme, particularly for slow waves. This is true with or without the use of high-resolution limiters.
- As the pressure-relaxation parameter in the Roe5 scheme is increased, the instantaneous-relaxation results are recovered. Instantaneous pressure relaxation annihilates the fastest waves, so that the solution approaches that of the four-equation system.
- It appears that the approach of two pressures and instantaneous pressure relaxation does not provide an easy way to overcome the problem of complex eigenvalues in the four-equation system.

## Acknowledgements

I am grateful to have received a doctoral fellowship from the Research Council of Norway.

Tore Flåtten of IRIS has provided several helpful suggestions regarding the calculations and the manuscript, and I am pleased to acknowledge them. Thanks are also due to my colleagues Erik B. Hansen and Robert Olsen, who have read the manuscript and given constructive comments.

The remarks of the referees contributed to improving the paper, and are appreciated.

## References

- Abgrall, R. How to prevent pressure oscillations in multicomponent flow calculations: A quasi conservative approach. *Journal of Computational Physics*, volume 125, no. 1: pages 150–160, April 1996.
- Abgrall, R. and Saurel, R. Discrete equations for physical and numerical compressible multiphase mixtures. *Journal of Computational Physics*, volume 186, no. 2: pages 361–396, April 2003.
- Baer, M. R. and Nunziato, J. W. A two-phase mixture theory for the deflagration-to-detonation transition (DDT) in reactive granular materials. *International Journal of Multiphase Flow*, volume 12, no. 6: pages 861–889, 1986.
- Bestion, D. The physical closure laws in the CATHARE code. *Nuclear Engineering and Design*, volume 124, no. 3: pages 229–245, December 1990.
- Chung, M.-S., Chang, K.-S. and Lee, S.-J. Numerical solution of hyperbolic two-fluid two-phase flow model with non-reflecting boundary conditions. *International Journal of Engineering Science*, volume 40, no. 7: pages 789–803, 2002.
- Coquel, F., El Amine, K., Godlewski, E., Perthame, B. and Rascle, P. A numerical method using upwind schemes for the resolution of two-phase flows. *Journal of Computational Physics*, volume 136, no. 2: pages 272–288, 1997.
- Cortes, J., Debussche, A. and Toumi, I. A density perturbation method to study the eigenstructure of two-phase flow equation systems. *Journal of Computational Physics*, volume 147, no. 2: pages 463–484, 1998.
- Drew, D. A. and Passman, S. L. *Theory of Multicomponent Fluids*, volume 135 of *Applied Mathematical Sciences*. Springer-Verlag, New York, 1999. ISBN 0-387-98380-5.

- Evje, S. and Flåtten, T. Hybrid flux-splitting schemes for a common two-fluid model. *Journal of Computational Physics*, volume 192, no. 1: pages 175–210, November 2003.
- Evje, S. and Flåtten, T. Hybrid central-upwind schemes for numerical resolution of two-phase flows. *ESAIM: Mathematical Modelling and Numerical Analysis*, volume 29, no. 2: pages 253–273, March–April 2005.
- Flåtten, T. *Hybrid flux splitting schemes for numerical resolution of two-phase flows*. Dr. ing. thesis, Norwegian University of Science and Technology, Department of Energy and Process Engineering, Trondheim, 2003. ISBN 82-471-5670-9.
- Harten, A. High resolution schemes for hyperbolic conservation laws. *Journal of Computational Physics*, volume 49, no. 3: pages 357–393, March 1983.
- Karni, S., Kirr, E., Kurganov, A. and Petrova, G. Compressible two-phase flows by central and upwind schemes. *ESAIM: Mathematical Modelling and Numerical Analysis*, volume 38, no. 3: pages 477–493, May–June 2004.
- Lallemand, M.-H., Chinnayya, A. and Le Metayer, O. Pressure relaxation procedures for multiphase compressible flows. *International Journal for Numerical Methods in Fluids*, volume 49, no. 1: pages 1–56, May 2005.
- LeVeque, R. J. *Finite Volume Methods for Hyperbolic Problems*. Cambridge University Press, Cambridge, UK, 2002. ISBN 0-521-00924-3.
- Munkejord, S. T. *Analysis of the two-fluid model and the drift-flux model for numerical calculation of two-phase flow*. Doctoral thesis, Norwegian University of Science and Technology, Department of Energy and Process Engineering, Trondheim, November 2005. ISBN 82-471-7338-7.
- Munkejord, S. T. Partially-reflecting boundary conditions for transient two-phase flow. *Communications in Numerical Methods in Engineering*, volume 22, no. 7: pages 781–795, July 2006.
- Munkejord, S. T. and Papin, M. The effect of interfacial pressure in the discrete-equation multiphase model. *Computers & Fluids*, volume 36, no. 4: pages 742–757, May 2007.
- Murrone, A. and Guillard, H. A five equation reduced model for compressible two phase flow problems. *Journal of Computational Physics*, volume 202, no. 2: pages 664–698, January 2005.
- Niu, Y.-Y. Advection upwinding splitting method to solve a compressible two-fluid model. *International Journal for Numerical Methods in Fluids*, volume 36, no. 3: pages 351–371, June 2001.

- Paillère, H., Corre, C. and García Cascales, J. R. On the extension of the AUSM+ scheme to compressible two-fluid models. *Computers & Fluids*, volume 32, no. 6: pages 891–916, July 2003.
- Ramshaw, J. D. and Trapp, J. A. Characteristics, stability, and short-wavelength phenomena in two-phase flow equation systems. *Nuclear Science and Engineering*, volume 66, no. 1: pages 93–102, 1978.
- Ransom, V. H. Faucet flow. In: G. F. Hewitt, J. M. Delhay and N. Zuber, editors, *Numerical Benchmark Tests*, volume 3 of *Multiphase Science and Technology*, pages 465–467. Hemisphere/Springer, Washington, USA, 1987. ISBN 0-89116-561-4.
- Ransom, V. H. and Hicks, D. L. Hyperbolic two-pressure models for two-phase flow. *Journal of Computational Physics*, volume 53, no. 1: pages 124–151, 1984.
- Roe, P. L. Approximate Riemann solvers, parameter vectors, and difference schemes. *Journal of Computational Physics*, volume 43, no. 2: pages 357–372, October 1981.
- Sainsaulieu, L. Finite-volume approximation of two phase-fluid flows based on an approximate Roe-type Riemann solver. *Journal of Computational Physics*, volume 121, no. 1: pages 1–28, October 1995.
- Saurel, R. and Abgrall, R. A multiphase Godunov method for compressible multifluid and multiphase flow. *Journal of Computational Physics*, volume 150, no. 2: pages 425–467, April 1999.
- Saurel, R. and LeMetayer, O. A multiphase model for compressible flows with interfaces, shocks, detonation waves and cavitation. *Journal of Fluid Mechanics*, volume 431: pages 239–271, March 2001.
- Soo, S. L. *Multiphase fluid dynamics*. Science Press, Beijing, 1990. ISBN 0-291-39781-6, 70-300-0102.
- Tiselj, I. and Petelin, S. Modelling of two-phase flow with second-order accurate scheme. *Journal of Computational Physics*, volume 136, no. 2: pages 503–521, 1997.
- Toro, E. F. *Riemann solvers and numerical methods for fluid dynamics*. Springer-Verlag, Berlin, second edition, 1999. ISBN 3-540-65966-8.
- Toumi, I. An upwind numerical method for two-fluid two-phase flow models. *Nuclear Science and Engineering*, volume 123, no. 2: pages 147–168, 1996.

- Toumi, I. and Kumbaro, A. An approximate linearized Riemann solver for a two-fluid model. *Journal of Computational Physics*, volume 124, no. 2: pages 286-300, March 1996.
- Trapp, J. A. and Riemke, R. A. A nearly-implicit hydrodynamic numerical scheme for two-phase flows. *Journal of Computational Physics*, volume 66, no. 1: pages 62-82, September 1986.
- van Leer, B. Towards the ultimate conservative difference scheme IV. New approach to numerical convection. *Journal of Computational Physics*, volume 23, no. 3: pages 276-299, 1977.